Rapid riparian ecosystem recovery in low-latitudinal North China following the end-Permian mass extinction

Wenwei Guo[1, 2], Li Tian[2*], Daoliang Chu[2], Wenchao Shu[2], Michael J. Benton[3], Jun Liu[4], Jinnan Tong[2]

[1]College of Culture and Tourism, Zhangzhou Institute of Technology, Zhangzhou 363000, People's Republic of China; [2]State Key Laboratory of Biogeology and Environmental Geology, China University of Geosciences, Wuhan, 430074, People's Republic of China; [3]School of Earth Sciences, University of Bristol, BS8 1RJ, UK; [4]Institute of Vertebrate Paleontology and Paleoanthropology, Chinese Academy of Sciences, Beijing 100044, People's Republic of China

***Author for Correspondence:** Li Tian, Email: tianlibgeg@cug.edu.cn

Abstract

The greatest mass extinction at the end of the Permian, ca. 252 million years ago, led to a tropical dead zone on land and sea. The speed of recovery of life has been debated, whether fast or slow, and terrestrial ecosystems are much less understood than marine. Here, we show fast reestablishment of riparian ecosystems in low-latitude North China as little as ~2 million years after the end-Permian mass extinction. The initial ichnoassemblages in shallow lacustrine and fluvial facies of late Smithian age are monospecific, devoid of infaunalization, with apparent size reduction. In the following Spathian, relatively complex, multi-level, structured riverain ecosystems had been rebuilt including medium-sized carnivores, plant stems, root traces, increased ichnological complexity, and significantly enhanced infaunalization. Specifically, burrowing behavior had re-emerged as a key life strategy not only to minimize stressful climatic conditions, but possibly to escape predation.

Introduction

The end-Permian mass extinction (EPME) is one of the most devastating bio-crises in the history of life and it destroyed both marine and terrestrial ecosystems (Wignall, 2015; Fan et al., 2020). A key feature of the EPME was the clearing of life from tropical ecosystems (e.g., Sun et al., 2012). Environmental extremes, especially lethal heat, largely flattened the tropical biodiversity peak, and marine animals were forced to migrated poleward or into deeper water (Liu et al., 2020; Song et al., 2020). Such effects were more brutal on land. A tropical “tetrapod gap”, spanning between 15°N and ~31°S, prevailed in the Early Triassic, or at particular intervals of intense global warming, even though the nature, temporal duration and spatial range of the Tropical Dead Zone (TDZ) remain

debated (Bernardi et al., 2018; Allen et al., 2020; Romano et al., 2020; Liu et al., 2022).

Long-term environmental perturbations after the EPME resulted in delayed recovery in the sea until the Middle Triassic (Chen and Benton, 2012), although several fast evolvers bounced back fast before being killed by further repeat hyperthermal events through the Early Triassic, as evidenced by the Guiyang Biota found ~1 million years (Myr) after the EPME (Dai et al., 2023). However, the post-extinction recovery on land has remained largely unclear. The taxonomic diversity of vertebrates may have re-flourished soon after the extinction in European Russia (Tverdokhlebov et al., 2003), but it apparently took longer, until the latest Early Triassic, in the Central European Basin (e.g., Scholze et al., 2017). Model results of tetrapod-dominated paleocommunities from the Karoo also displayed a short lived, unstable ecosystem during the Early Triassic *Lystrosaurus* Assemblage Zone, before being replaced by a globally stable ecological structure established in the Middle Triassic (Roopnarine et al., 2019; Viglietti et al., 2022). It seemed that plants showed a quick return in Australia (Vajda and Kear, 2024), yet reorganization of floral communities was hindered by repeated climatic stressors, such as the Smithian–Spathian warming event (Mays et al., 2020; Vajda et al., 2020). Likewise, the initial construction of the mesophytic flora was in the earliest Middle Triassic in North China (Shu et al., 2022).

Other body fossils, especially non-marine invertebrates, are relatively scarce in the post-extinction interval. The earliest Middle Triassic riverine community, consisting of insects, rare fishes and trace fossils in equatorial western peri-Tethys (Baucon et al., 2014; Mujal et al., 2017; Matamales-Andreu et al., 2021) and the Anisian–Ladinian deep lake biota, comprising diverse insects, fishes, fish coprolites and plants of North China (Zhao et al., 2020), were thought to be representative of recovered terrestrial ecosystems in tropical after the EPME. However, recent

studies have revealed that biodiversity was not as low as expected in North China from the ichnological point of view, because relatively diverse trace fossils have been found in upper Lower Triassic deposits with moderate bioturbation (Guo et al., 2019; Xing et al., 2021; Zheng et al., 2021). Here, we report an unexpectedly rapidly recovered ecosystem from the TDZ after the EPME, based on compiled data of vertebrates, invertebrate trace fossils, and plant remains from Lower Triassic successions and outcrops in North China, to show how animals survived in harsh conditions and how the ecosystems finally recovered from the mass extinction event in latitudinal terrestrial settings.

Geological Settings and Methods

Abundant trace fossils have been identified from the uppermost Permian–Lower Triassic of the Shichuanhe, Dayulin, Liulin sections and Hongyatou, Tuncun, Mafang outcrops in the Central North China Basin (Fig. 1). During the early Mesozoic, the North China Block was located at about 20°N based on paleomagnetic reconstruction (Huang et al., 2018; Guo et al., 2022). The Permo-Triassic strata, typically terrestrial red-beds, comprising the Sunjiagou, Liujiagou, Heshanggou (HSG) and Ermaying formations in ascending order, display varied depositional environments from fluvial to lacustrine facies (See Figure S1 and Table S1 in the Supporting Information). The Sunjiagou Formation mainly consists of red massive siltstone and intercalated sandstone of varied thickness, and paleosols and trace fossils were locally developed, demonstrating floodplain to lakeshore facies (Ji et al., 2022; Yu et al., 2022). The Liujiagou Formation is characterized by thick cross-bedded sandstones and intraclast conglomerates. Lenticular sand bodies and erosive bases of sandstones are common in the lower part, indicating fluvial channel facies under braided river systems (Zhu et al., 2019; Ji et al., 2022). Interlayered thick siltstones of lakeshore facies increase upwards, accompanied

by weak evidence of biological activity. The HSG is dominated by massive siltstones, with multi-layered paleosols, diverse trace fossils and some plant remains, belonging to alluvial plain and lakeshore facies, with periodic aerial exposure (Zhu et al., 2020; Ji et al., 2022).

Recently, a U-Pb CA-ID-TIMS age calibrated magnetostratigraphy from the Shichuanhe section provided a basic geochronological timescale for the fossil-poor strata in North China (Guo et al., 2022; Figure S2). Accordingly, the Permian–Triassic Boundary is constrained in the upper part of the Sunjiagou Formation based on the age of 252.21 ± 0.15 million years ago (Ma), with the base of the Smithian and Spathian being roughly located in the lower and upper Liujiagou Formation respectively. However, loss of several magnetozones in a regional hiatus makes it difficult to place the Lower–Middle Triassic Boundary precisely, which was tentatively put at the lithological contact of the HSG and the overlying Ermaying Formation (Guo et al., 2022). The 245–247 Ma ages from tuff layers at the base of the Ermaying Formation roughly support this correlation (Zhu et al., 2022).

In order to discriminate the recovery stages, several ichno-ecological criteria are used. Both bioturbation index (BI) and ichnofabric index (ii), which have been critically reviewed by Luo et al. (2020), are used to quantify bioturbation intensity. Values of ii and BI, ranging from 1–6 and 0–6, respectively, co-indicate the gradual increase of biotic disturbance from no bioturbation to total homogenization of sediments. Ichnodiversity represents the number of ichnotaxa, but it is not strictly equivalent to biodiversity, as a certain trace can be made by different animals and multiple trace types can originate from a single taxon (Luo et al., 2019). Ichnodisparity emphasizes the variability of architectural designs of trace fossils (Buatois et al., 2017), morphiologically distinct forms being termed ichnomorphs. Therefore, both ichnodiversity and ichnodisparity are employed to assess the behavioral responses of animals and the stage of infaunal biotic recovery (Table S2–4). Size and

penetration depth are also measured in places that can represent the average level of each burrow. Tiering, referring to the life position of an animal vertically in the sediment, is divided into surficial, semi-infaunal (0–0.5 cm), shallow (0.5–6 cm), intermediate (6–12 cm) and deep infaunal tiers (> 12 cm), based on Minter et al. (2017).

Thin sections of plant stem specimens were prepared to examine vertical and cross-sectional microstructures. Meanwhile, Micro-CT scanning (SkyScan 1172 X-ray; State Key Laboratory of Biogeology and Environmental Geology) was employed to reconstruct the internal structures of stems.

Results and Discussion

Infaunal Crisis and Living Strategy after the EPME in North China

An infaunal crisis, marked by the disappearance of the moderately diversified pre-extinction ichnofauna and the absence of biogenic structures, is identified in successions of late Changhsingian–early Smithian age. The latest Permian floodplain facies were mainly occupied by shallow–intermediate tiers of freely motile non-specialized deposit-feeding animals (Figure 1), akin to the Paleozoic suites reported before (Minter et al., 2017). Both ichnodiversity and ichnodisparity declined abruptly in the middle Sunjiagou Formation (near the 252.21 Ma aged tuff layer), following a prolonged non-bioturbated interval (Guo et al., 2019, 2022; Xing et al., 2021). The infaunal crisis was contemporary with the extirpation of the pareiasaur fauna (*Shihtienfenia*) and deforestation of the youngest Palaeozoic *Ullmannia-Pseudovoltzia-Germaropteris* assemblage in North China, representing the EPME on land (Liu et al., 2022; Shu et al., 2022).

The early recovery ichnofauna preserved in the upper Liujiagou Formation, about late Smithian

in age, was short-lived. This lakeshore ichnofauna, including seven ichnogenera of six ichnomorphs, is characterized by surficial and semi-infaunal tiered simple burrows or trails, with rare trackways and root traces, which weakly disturbed the sediments (Figure S3). Dwarfism in trace makers is observed from all ichnogenera, with burrow sizes reduced from a mean of 4.06 mm before the EPME (n = 779) to 2.06 mm (n = 341) in the late Smithian (Figure 4 and Figure S7), and as seen in individual ichnogenera such as *Kouphichnium* (Shu et al., 2018). The depauperate ichnofauna of the late Smithian was monospecific, representing initial recolonization of empty niches by opportunists. However, recurrent occurrences of microbial induced sedimentary structures (MISS) in the Liujiagou Formation show that depressed ecosystems persisted into the Smithian (Tu et al., 2016; Chu et al., 2017). Earlier work has shown that increases in microbial abundance were generally associated with hyperthermal events, the principal causee for mass extinction on land (Mays et al., 2021). Accumulations of microbes were favored by low dissolved oxygen concentration conditions and their secondary metabolites could also be toxic to animals (Pacton et al., 2011; Paerl and Otten, 2013). Therefore, repeated thriving of MISS during the Dienerian–Smithian interval disrupted ecological stability in freshwater ecosystems and delayed biotic recovery.

Abundant trace fossils are identified in the Spathian HSG Formation, comprising 16 ichnogenera of nine ichnomorphs, and two informally designated types (Figure 2 and Figure S4–5). This morphologically complex ichnofauna was dominated by actively filled burrows, with few arthropod trackways, which were probably produced by decapod crustaceans, myriapods and insects (Table S5). The lakeshore and alluvial plain facies were occupied by multi-tiered traces, including surficial trackways (e.g., *Diplichnites*; *Kouphichnium*), semi-infaunal (e.g., *Helminthoidichnites*; *Gordia*), shallow (e.g., *Palaeophycus*; *Scoyenia*), intermediate (e.g., *Taenidium*) and deep tiers

(*Camborygma*; *Skolithos*; Figure 1c). Trace producers that colonized varied ecospace and shallower tiers are generally crosscut by deeper penetrative burrows (Figure 2a), resulting in moderately to substantially bioturbated deposits, with ii 2–3 and BI 3–4 at most layers. In several horizons, the uppermost few centimeters of sediments are totally obliterated, mostly by the activity of deposit feeding animals. However, distal terminal fan facies are weakly reworked by simple traces such as *Skolithos* and *Palaeophycus* or root traces. Additionally, average burrow sizes of all ichnogenera also increased to 3.9 mm in the HSG (n = 2241, Figure 4 and Figure S7–8).

Several large burrows in the Spathian indicate the occurrence of advanced ecosystem engineers. *Camborygma litonomos* were found in the basal HSG of the Shichuanhe section and outcrop in Hongyatou, co-occurring with *in situ* preserved *Neocalamites* plant fossils, and other traces, such as *Diplichnites*, *Monomorphichnus* and *Skolithos* (Figure S6). Surfaces of *C. litonomos* were occasionally intertwined with rhizotubules (Figure 2l), suggesting that those plants could be important constituents in the diet of crayfish or that the crayfish might have hidden among the roots. In addition, another large burrow was identified in the Liulin section; this sub-horizontal unbranched burrow displays probable longitudinal scratch marks on the external surface, but poor preservation and limited specimens hinder a definite designation (Figure S5). ?*Beaconites*, found in the lower part of the HSG at Mafang, are characterized by meniscate structures (Figure 2o–p and Figure S5C–E), akin to those of large *Beaconites* from breccia facies in the Devonian red sandstone of Britain (Brück, 1987). Although the biological nature of these large burrows cannot be confirmed, their activities increased biogenic reworking of sediment and soils, improved geochemical recycling and ecosystem complexity in the Spathian, implying key roles in ecosystem functioning.

Although climatic and environmental conditions in the early Spathian were still not cool and

wet enough for thriving and abundant life, a fossorial strategy would have been useful for terrestrial animals to avoid heat and aridity. Midday temperatures > 35°C, as occurred during peaks of global warming at the EPME and at points through the Early Triassic, cannot be tolerated for long by terrestrial (or aquatic) animals (Benton, 2018; Liu et al., 2022). The increase in tetrapod burrow abundance and complexity in the Lower Triassic suggest that a fossorial lifestyle allowed tetrapods to endure harsh post-extinction environmental conditions (Marchetti et al., 2024). Likewise, we envisage that infaunalization could also have been a vital strategy for invertebrates to survive and thrive. More intensively occupied ecospace in the late Spathian, characterized by increased burrowing and complicated crosscutting relations among ichnogenera, may indicate an adaptive response to heightened predation pressure or competition for available resources.

Fast recovered terrestrial ecosystem in tropical region

Our results also shed light on the timing of the TDZ. The late Smithian-age ichnofauna, although impoverished, represents early opportunist-dominated communities that explore empty ecospace under inhospitable environments, which constrain persistence of the TDZ to the late Smithian in North China. Newly discovered tetrapods from the HSG provide crucial insights into Spathian aged ecosystems. Historically, vertebrates found in this lithological unit were exclusively from its middle–upper portions (Li et al., 2008; Figure 3-4). The presence of Archosauromorpha (e.g., *Fugusuchus*; Fig. 3c) and Procolophonomorpha (e.g., *Eumetabolodon*; Fig. 3d) could reflect their tolerance to hot and arid condition, while the initial diversification of archosauromorphs in the Olenekian was interpreted as a response to empty ecological space after the EPME (McLoughlin et al., 2020; Romano et al., 2020). Herein, a cluster of tetrapod skeletons, including a few articulated

bones, were found near the base of HSG (early Spathian; Figure 3i). Body trunk lengths are estimated at 30–40 cm for the vertebrates, and the postcranial skeleton suggests a carnivorous feeding strategy. Although the specimens are not yet fully prepared for taxonomic description, they clearly show the existence of tetrapods at this level, narrowing the "tetrapod gap" to the Spathian.

Plants, as key components of the ecosystem, were patchily distributed in the Early Triassic (Shu et al., 2022). However, root traces (rhizoliths) are quite abundant, especially in the Dayulin section (Figure 2d and Figure S6). The different styles of preservation and various morphologies of rhizoliths provide information about the moderately to relatively well-drained red paleosols in alluvial plain facies (Kraus and Hasiotis, 2006). Specifically, *in situ* preserved vertical *Neocalamites* stems and *Pleuromeia* found in the lower HSG of the Shichuanhe and Hongyatou sections both occur in tandem with crayfish trace fossils and other burrows.

Delayed terrestrial recovery was proposed based on the Tongchuan fauna from North China, which consisted of diverse insects, ostracods, fishes, etc, signalling a fully recovered deep lake ecosystem in the Middle Triassic, i.e., ~8–12 Myr after the EPME (Zheng et al., 2018; Zhao et al., 2020). However, compiled paleontological data herein show that ecosystems on land occurred in tropical regions as early as in the Spathian, ~2 Myr after the EPME (Figure S9). The enhanced floral coverage attributed to different types of roots and plant fossils had great impact on the initiation of a post-EPME ecosystem, especially the co-occurring stems and trace fossils, which suggest that riverain realms might have been refugia for the survival and evolution of the Spathian biota (Figure 5). Increased abundance and quantity of faunal communities can be inferred from ichnodiversity, with possible candidate trace-producers including limuloids, crayfishes, spinicaudatans, insects and even small-sized vertebrates (Table S5), and moderate bioturbation made by high-density resting

traces, respectively. Coeval tetrapods, despite being rare, do show the existence of carnivores and further complexity in local ecological structures. Reconstruction of freshwater ecosystems in the Spathian was also facilitated by amelioration of the climate (Figure 4). Paleosol-based paleoclimatic reconstructions suggest that precipitation was ~520–680 mm/y in the late Spathian, with pCO_2 estimated from paleosols at 1523 ± 417 ppm (Joachimski et al., 2022; Yu et al., 2022), indicating mitigation of hyperthermal conditions. Geochemical proxies of weathering intensity, salinity and clayiness, along with increased hygrophyte/xerophyte ratio, also demonstrate the transition to wetter conditions (Shu et al., 2022; Zhu et al., 2022).

Conclusions

The diverse community of the HSG Formation, consisting of tetrapods, plant stems, rhizoliths, and diverse ichnofossils suggests a rapid recovery of life in low-latitudinal terrestrial environments in the Spathian, as little as ~2 Myr after the end-Permian biotic crisis. The newly discovered vertebrate fossils are medium-sized carnivores of approximately early Spathian age, representing the earliest Triassic-aged tetrapods found in North China. High ichnodiversity and ichnodisparity, and three types of large burrows, not only results in intensified bioturbation, but provide additional information about the enriched local biota. Furthermore, enhanced burrowing behavior is considered a key survival-recovery strategy to adapt to harsh climatic and environmental conditions on land. The co-occurring trace fossils and stems, and coeval tetrapod in alluvial plain facies, suggesting that the riverain regions could be refugia for the reorganization of post-EPME ecosystem.

Data Availability Statement

All supplementary data related to this paper is available in the end of this manuscript.

Article and author information

Author details

Wenwei Guo

- College of Culture and Tourism, Zhangzhou Institute of Technology, Zhangzhou, People's Republic of China
- State Key Laboratory of Biogeology and Environmental Geology, School of Earth Science, China University of Geosciences, Wuhan, People's Republic of China

Contribution: Conceptualization; Methodology; Validation; Formal analysis; Investigation; Data curation; Writing–original draft preparation; Writing–review & editing; Visualization

Competing interests: No competing interests declared

Li Tian

State Key Laboratory of Biogeology and Environmental Geology, School of Earth Science, China University of Geosciences, Wuhan, People's Republic of China

Contribution: Conceptualization; Methodology; Validation; Formal analysis; Investigation; Data curation; Writing–original draft preparation; Writing–review & editing; Visualisation; Project administration; Funding acquisition

For correspondence: tianlibgeg@cug.edu.cn

Competing interests: No competing interests declared

Daoliang Chu

State Key Laboratory of Biogeology and Environmental Geology, School of Earth Science, China University of Geosciences, Wuhan, People's Republic of China

Contribution: Conceptualization; Methodology; Validation; Investigation; Data curation; Writing–original draft preparation; Writing–review & editing; Visualization; Project administration; Funding acquisition

Competing interests: No competing interests declared

Wenchao Shu

State Key Laboratory of Biogeology and Environmental Geology, School of Earth Science, China University of Geosciences, Wuhan, People's Republic of China

Contribution: Methodology; Validation; Formal analysis; Investigation; Writing–original draft preparation; Writing–review & editing; visualization

Competing interests: No competing interests declared

Michael J. Benton

School of Earth Sciences, University of Bristol, UK

Contribution: Conceptualization; Methodology; Validation; Formal analysis; Investigation; Writing–review & editing; Visualization; Funding acquisition

Competing interests: No competing interests declared

Jun Liu

Institute of Vertebrate Paleontology and Paleoanthropology, Chinese Academy of Sciences, Beijing, People's Republic of China

Contribution: Conceptualization; Methodology; Validation; Formal analysis; Investigation; Writing–review & editing; Visualization; Funding acquisition

Competing interests: No competing interests declared

Jinnan Tong

State Key Laboratory of Biogeology and Environmental Geology, School of Earth Science, China University of Geosciences, Wuhan, People's Republic of China

Contribution: Conceptualization; Validation; Formal analysis; Investigation; Writing–review & editing; Visualization; Supervision; Project administration; Funding acquisition

Competing interests: No competing interests declared

Acknowledgments

We thank Kaixuan Ji, Gan Liu and Yuyang Wu for assisting in the field. We also thank the editor and anonymous reviewers for their comments and constructive suggestions. This work was supported by the National Natural Science Foundation of China (grant nos. 42030513) to L. T., D. C. and J. T., the Strategic Priority Research Program of the Chinese Academy of Sciences (grant no. XDB26000000) to J. L. and the Natural Environment Research Council (UK) of grant no. NE/P013724/1 to M. J. B.

References

Allen BJ, Wignall PB, Hill DJ, Saupe EE, Dunhill AM. 2020. The latitudinal diversity gradient of tetrapods across the Permo-Triassic mass extinction and recovery interval. *Proceedings of the Royal Society B*, **287**: 20201125. https://doi.org/10.1098/rspb.2020.1125

Baucon A, Ronchi A, Felletti F, Neto de Carvalho C. 2014. Evolution of crustaceans at the edge of the end-Permian crisis: Ichnonetwork analysis of the fluvial succession of Nurra (Permian–Triassic, Sardinia, Italy). *Palaeogeography*, *Palaeoclimatology*, *Palaeoecology*, **410**: 74–103. https://doi.org/10.1016/j.palaeo.2014.05.034

Benton MJ. 2018. Hyperthermal-driven mass extinctions: killing models during the Permian–Triassic mass extinction. *Philosophical Transactions of the Royal Society A*, **376**: 20170076. https://doi.org/10.1098/rsta.2017.0076

Bernardi M, Petti FM, Benton MJ. 2018. Tetrapod distribution and temperature rise during the Permian-Triassic mass extinction. *Proceedings of the Royal Society B*, **285**: 20172331. https://doi.org/10.1098/rspb.2017.2331

Brück PM. 1987. A note on the trace fossil *Beaconites barretti* in the Old Red Sandstone of County Dublin, Ireland. *Proceedings of the Geologists' Association*, **98**: 259–263. https://doi.org/10.1016/S0016-7878(87)80043-3

Buatois LA, Wisshak M, Wilson MA, Mángano MG, 2017. Categories of architectural designs in trace fossils: a measure of ichnodisparity. *Earth-Science Reviews*, **164**: 102–181. https://doi.org/10.1016/j.earscirev.2016.08.009

Buatois LA, Borruel-Abadía V, De la Horra R, Galán-Abellán AB, López-Gómez J, Barrenechea JF, Arche A. 2021. Impact of Permian mass extinctions on continental invertebrate infauna. *Terra Nova*, **33**: 455–464. https://doi.org/10.1111/ter.12530.

Chen ZQ, Benton MJ. 2012. The timing and pattern of biotic recovery following the end-Permian mass extinction. *Nature Geoscience*, **5**: 375–383. https://doi.org/10.1038/ngeo1475

Chu DL, Tong JN, Bottjer DJ, Song HJ, Song HY, Benton MJ, Tian Li, Guo WW. 2017. Microbial mats in the terrestrial Lower Triassic of North China and implications for the Permian–Triassic mass extinction. *Palaeogeography, Palaeoclimatology, Palaeoecology*, **474**: 214–231. https://doi.org/10.1016/j.palaeo.2016.06.013

Dai X, Davies JHFL, Yuan Z, Brayard A, Ovtcharova M, Xu GH, Liu XK, Smith CPA, Schweitzer CE, Li MT, Perrot MG, Jiang SY, Miao LY, Cao YR, Yan J, Bai RY, Wang FY, Guo W, Song HY, Tian L, Dal Corso J, Liu YT, Chu DL, Song HJ. 2023. A Mesozoic fossil lagerstätte from 250.8 million years ago shows a modern-type marine ecosystem. *Science*, **379**: 567–572. DOI: 10.1126/science.adf1622

Fan JX, Shen SZ, Erwin DH, Sadler PM, MacLeod N, Cheng QM, Hou XD, Yang J, Wang XD, Wang Y, Zhang H, Chen X, Li GX, Zhang YC, Shi YK, Yuan DX, Chen Q, Zhang LN, Li C, Zhao YY. 2020. A high-resolution summary of Cambrian to early Triassic marine invertebrate biodiversity. *Science*, **367**: 272–277. DOI: 10.1126/science.aax4953

Guo WW, Tong JN, Tian L, Chu DL, Bottjer DJ, Shu WC, Ji KX. 2019. Secular variations of ichnofossils from the terrestrial Late Permian-Middle Triassic succession at the Shichuanhe section in Shaanxi Province, North China. *Global and Planetary Change*, **181**: 102978. https://doi.org/10.1016/j.gloplacha.2019.102978

Guo WW, Tong JN, He Q, Hounslow MW, Song HY, Dal Corso J, Wignall PB, Ramezani J, Tian L, Chu DL. 2022. Late Permian–Middle Triassic magnetostratigraphy in North China and its implications for terrestrial-marine correlations. *Earth and Planetary Science Letters*, **585**:

117519. https://doi.org/10.1016/j.epsl.2022.117519

Huang BC, Yan Y, Piper JDA, Zhang D, Yi Z, Yu S, Zhou T. 2018. Paleomagnetic constraints on the paleogeography of the East Asian blocks during Late Paleozoic and Early Mesozoic times. *Earth-Science Reviews*, **186**: 8–36. https://doi.org/10.1016/j.earscirev.2018.02.004

Ji K, Wignall PB, Tong JN, Yu YY, Guo WW, Shu WC, Chu DL. 2022. Sedimentology of the latest Permian to Early Triassic in the terrestrial settings of the North China Basin: Low-latitude climate change during a warming-driven crisis. *Geological Society of America Bulletin*, **135**: 481-503. https://doi.org/10.1130/b36260.1

Joachimski MM, Müller J, Gallagher TM, Mathes G, Chu DL, Mouraviev F, Silantiev V, Sun YD, Tong JN. 2022. Five million years of high atmospheric CO_2 in the aftermath of the Permian-Triassic mass extinction. *Geology*, **50**: 650–654. https://doi.org/10.1130/G49714.1

Kraus MJ, Hasiotis ST. 2006. Significance of different modes of rhizolith preservation to interpreting paleoenvironmental and paleohydrologic settings: Examples from Paleogene paleosols, Bighorn Basin, Wyoming, U.S.A. *Journal of Sedimentary Research*, **76**: 633–646. https://doi.org/10.2110/jsr.2006.052

Li JL, Wu X, Zhang F. 2008. *The Chinese Fossil Reptiles and Their Kin*. Science Press, Beijing.

Liu J, Abdala F, Angielczyk KD, Sidor CA. 2022. Tetrapod turnover during the Permo-Triassic transition explained by temperature change. *Earth-Science Reviews*, **224**: 103886. https://doi.org/10.1016/j.earscirev.2021.103886.

Liu XK, Song HJ, Bond DPG, Tong JN, Benton MJ. 2020. Migration controls extinction and survival patterns of foraminifers during the Permian-Triassic crisis in South China. *Earth-Science Reviews*, **209**: 103329. https://doi.org/10.1016/j.earscirev.2020.103329

Luo M, Shi GR, Buatois LA, Chen ZQ. 2020. Trace fossils as proxy for biotic recovery after the end-Permian mass extinction. A critical review. *Earth-Science Reviews*, **203**: 103059. https://doi.org/10.1016/j.earscirev.2019.103059

Matamales-Andreu R, Penalver E, Mujal E, Oms O, Scholze F, Juarez J, Galobart A, Fortuny J. 2021. Early-Middle Triassic fluvial ecosystems of Mallorca (Balearic Islands): Biotic communities and environmental evolution in the equatorial western peri-Tethys. *Earth-Science Reviews*, **222**: 103783. https://doi.org/10.1016/j.earscirev.2021.103783

Marchetti L, MacDougall MJ, Buchwitz M, Canoville A, Herde M, Kammerer CF, Fröbisch J. 2024. Origin and early evolution of vertebrate burrowing behaviour. *Earth-Science Reviews*, **250**: 104702. https://doi.org/10.1016/j.earscirev.2024.104702

Mays C, Vajda V, Frank TD, Fielding CR, Nicoll RS, Tevyaw AP, McLoughlin S. 2020. Refined Permian–Triassic floristic timeline reveals early collapse and delayed recovery of south polar terrestrial ecosystems. *Geological Society of America Bulletin*, **132**: 1489–1513. https://doi.org/10.1130/B35355.1

Mays C, McLoughlin S, Frank TD, Fielding CR, Slater SM, Vajda V. 2021. Lethal microbial blooms delayed freshwater ecosystem recovery following the end-Permian extinction. *Nature Communications*, **12**: 5511. https://doi.org/10.1038/s41467-021-25711-3

McLoughlin S, Mays C, Vajda V, Bocking M, Frank TD, Fielding CR. 2020. Dwelling in the dead zone—Vertebrate burrows immediately succeeding the end-Permian extinction event in Australia. *Palaios*, **35**: 342-357. https://doi.org/10.2110/palo.2020.007

Minter NJ, Buatois LA, Mángano MG, Davies NS, Gibling MR, MacNaughton RB, Labandeira CC. 2017. Early bursts of diversification defined the faunal colonization of land. *Nature Ecology &*

Evolution, **1**: https://doi.org/10.1038/s41559-017-0175

Mujal E, Fortuny J, Bolet A, Oms O, López JÁ. 2017. An archosauromorph dominated ichnoassemblage in fluvial settings from the late Early Triassic of the Catalan Pyrenees (NE Iberian Peninsula). *PLoS One*, **12** (4): e0174693. http://dx.doi.org/10.1371/journal.pone.0174693

Pacton M, Gorin GE, Vasconcelos C. 2011. Amorphous organic matter—Experimental data on formation and the role of microbes. *Review of Palaeobotany and Palynology*, **166**: 253–267. https://doi.org/10.1016/j.revpalbo.2011.05.011

Paerl HW, Otten TG. 2013. Harmful cyanobacterial blooms: causes, consequences, and controls. *Microbial Ecology*, **65**: 995–1010. https://doi.org/10.1007/s00248-012-0159-y

Romano M, Bernardi M, Petti FM, Rubidge B, Hancox J, Benton MJ. 2020. Early Triassic terrestrial tetrapod fauna: a review. *Earth-Science Reviews*, **210**: 103331. https://doi.org/10.1016/j.earscirev.2020.103331

Roopnarine PD, Angielczyk KD, Weik A, Dineen A. 2019. Ecological persistence, incumbency and reorganization in the Karoo Basin during the Permian-Triassic transition. *Earth-Science Reviews*, **189**: 244−263. https://doi.org/10.1016/j.earscirev.2018.10.014

Scholze F, Wang Z, Kirscher U, Kraft J, Schneider JW, Götz AE, Joachimski MM, Bachtadse V. 2017. A multistratigraphic approach to pinpoint the Permian-Triassic boundary in continental deposits: the Zechstein–Lower Buntsandstein transition in Germany. Global and Planetary Change, **152**: 129–151. http://dx.doi.org/10.1016/j.gloplacha.2017.03.004

Shu WC, Tong JN, Tian L, Benton MJ, Chu DL, Yu JX, Guo WW. 2018. Limuloid trackways from Permian–Triassic continental successions of North China. *Palaeogeography*, *Palaeoclimatology*,

Palaeoecology, **508**: 71–90. https://doi.org/10.1016/j.palaeo.2018.07.022

Shu WC, Tong JN, Yu JX, Hilton J, Benton MJ, Shi X, Diez JB, Wignall PB, Chu DL, Tian L, Yi, ZX, Mao YD. 2022. Permian−Middle Triassic floral succession in North China and implications for the great transition of continental ecosystems. *Geological Society of America Bulletin*, **135**: 1747–1767. https://doi.org/10.1130/B36316.1

Song HJ, Huang S, Jia EH, Dai X, Wignall PB, Dunhill AM. 2020. Flat latitudinal diversity gradient caused by the Permian-Triassic mass extinction. *Proceedings of the National Academy of Sciences of the United States of America*, **117**: 17578–17583. https://doi.org/10.1073/pnas.1918953117

Sun YD, Joachimski MM, Wignall PB, Yan CB, Chen YL, Jiang HS, Wang LN, Lai XL. 2012. Lethally hot temperatures during the Early Triassic greenhouse. *Science*, **338**: 366–370. DOI:10.1126/science.1224126

Tu CY, Chen ZQ, Retallack GJ, Huang Y, Fang Y. 2016. Proliferation of MISS-related microbial mats following the end-Permian mass extinction in terrestrial ecosystems: Evidence from the Lower Triassic of the Yiyang area, Henan Province, North China. *Sedimentary Geology*, **333**: 50−69. https://doi.org/10.1016/j.sedgeo.2015.12.006

Tverdokhlebov VP, Tverdokhlebova GI, Surkov MV, Benton MJ. 2003. Tetrapod localities from the Triassic of the SE of European Russia. *Earth-Science Reviews*, **60**: 1–66. https://doi.org/10.1016/S0012-8252(02)00076-4

Vajda V, McLoughlin S, Mays C, Frank TD, Fielding CR, Tevyaw A, Lehsten V, Bocking M, Nicoll RS. 2020. End-Permian (252 Mya) deforestation, wildfires and flooding – an ancient biotic crisis with lessons for the present. *Earth and Planetary Science Letters*, **529**: 115875.

https://doi.org/10.1016/j.epsl.2019.115875

Vajda V, Kear BP. 2024. An earliest Triassic riparian ecosystem from the Bulgo Sandstone (Sydney Basin), Australia: palynofloral evidence of a high-latitude terrestrial vertebrate habitat after the end-Permian mass extinction. *Alcheringa: An Austalasian Journal of Palaeontology*, 1−12. https://doi.org/10.1080/03115518.2024.2392489

Viglietti PA, Rojas A, Rosvall M, Klimes B, Angielczyk KD. 2022. Network-based biostratigraphy for the late Permian to mid-Triassic Beaufort Group (Karoo Supergroup) in South Africa enhances biozone applicability and stratigraphic correlation. *Palaeontology*, **65**: e12622. https://doi.org/10.1111/pala.12622

Wignall PB. 2015. *The Worst of Times: How Life on Earth Survived Eighty Million Years of Extinction*. Princeton University Press, NJ: Princeton.

Xing ZF, Lin J, Fu YX, Zheng W, Liu YL, Qi YA. 2021. Trace fossils from the Lower Triassic of North China — a potential signature of the gradual recovery of a terrestrial ecosystem. *Palaeoworld*, **30**: 95–105. https://doi.org/10.1016/j.palwor.2020.06.002

Yu YY, Tian L, Chu DL, Song HY, Guo WW, Tong JN. 2022. Latest Permian–Early Triassic paleoclimatic reconstruction by sedimentary and isotopic analyses of paleosols from the Shichuanhe section in central North China Basin. *Palaeogeography, Palaeoclimatology, Palaeoecology*, **585**: 110726. https://doi.org/10.1016/j.palaeo.2021.110726

Zhao XD, Zheng DR, Xie GW, Jenkyns HC, Guan CG, Fang Y, He J, Yuan XQ, Xue NH, Wang H, Li S, Jarzembowski, EA, Zhang HC, Wang B. 2020. Recovery of lacustrine ecosystems after the end-Permian mass extinction. *Geology*, **48**: 609–613. https://doi.org/10.1130/G47502.1

Zheng DR, Chang SC, Wang H, Fang Y, Wang J, Feng CQ, Xie GW, Jarzembowski EA, Zhang HC,

Wang B. 2018. Middle-Late Triassic insect radiation revealed by diverse fossils and isotopic ages from China. *Science Advances*, **4**: eaat1380. https://doi.org/10.1126/sciadv.aat1380

Zheng W, Wan EZ, Xu X, Li D, Dai MY, Qi YA, Xing ZF, Liu YL. 2021. The variations of terrestrial trace fossils and sedimentary substrates after the end-Permian extinction in the Dengfeng area, North China. *Geological Journal*, **58**: 1223–1238. https://doi.org/10.1002/gj.4657

Zhu ZC, Liu YQ, Kuang HW, Benton MJ, Newell AJ, Xu H, An W, Ji SA, Xu SC, Peng N, Zhai QG. 2019. Altered fluvial patterns in North China indicate rapid climate change linked to the Permian-Triassic mass extinction. *Scientific Reports*, **9**: 16818. https://doi.org/10.1038/s41598-019-53321-z

Zhu ZC, Kuang HW, Liu YQ, Benton MJ, Newell AJ, Xu H, An W, Ji SA, Xu SC, Peng N, Zhai QG. 2020. Intensifying aeolian activity following the end-Permian mass extinction: Evidence from the Late Permian–Early Triassic terrestrial sedimentary record of the Ordos Basin, North China. *Sedimentology*, **67**: 2691-2720. https://doi.org/10.1111/sed.12716

Zhu ZC, Liu YQ, Kuang HW, Newell AJ, Peng N, Cui MM, Benton MJ. 2022. Improving paleoenvironment in North China aided Triassic biotic recovery on land following the end-Permian mass extinction. *Global and Planetary Change*, **216**: 103914. https://doi.org/10.1016/j.gloplacha.2022.103914

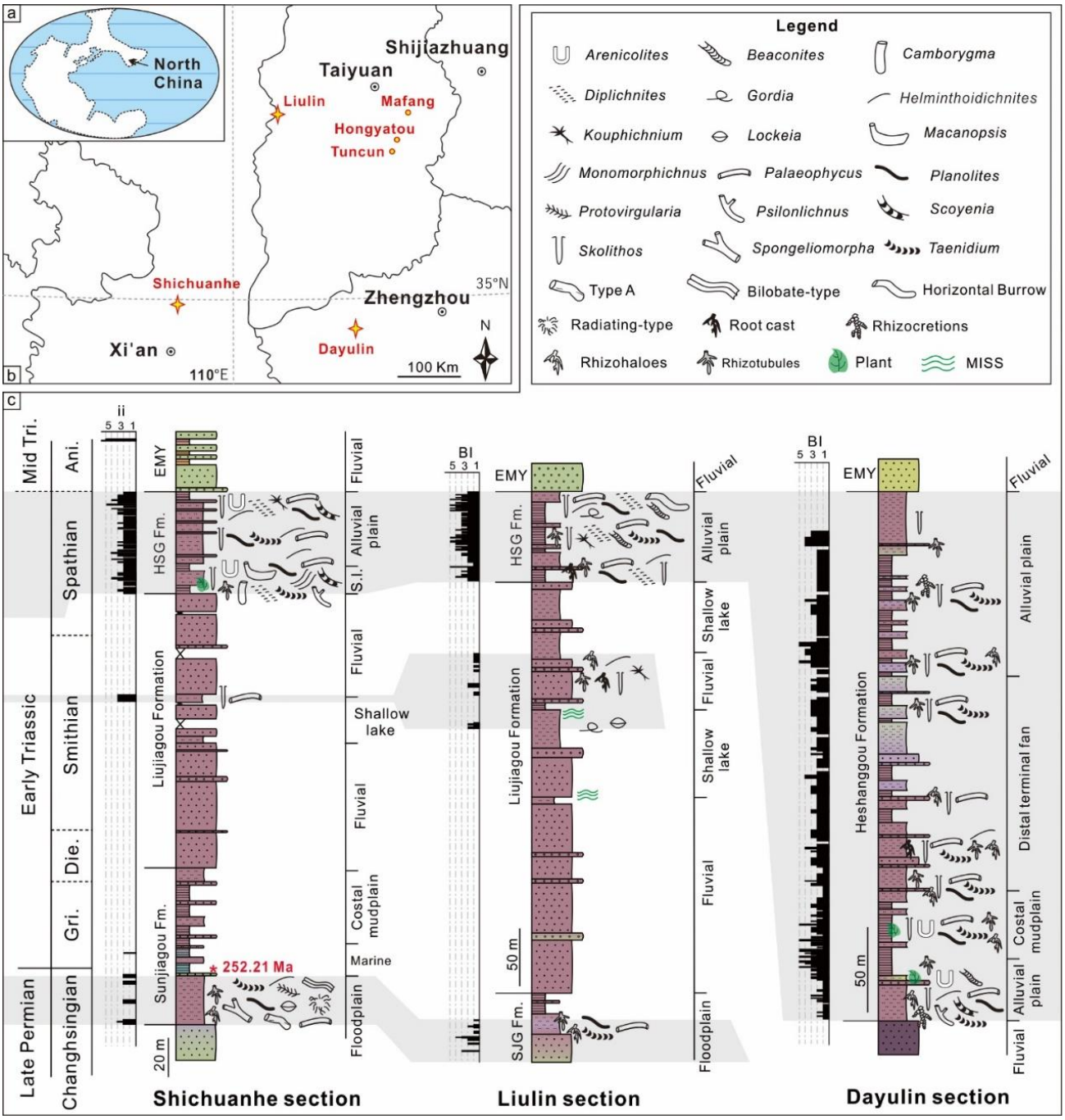

Figure 1. Location of the studied regions and lithological columns. (a–b) Permian-Triassic paleogeographic map of North China and the studied successions (stars) and outcrops (points). Base map is modified from Sun et al. (2012). (c) Depositional facies and detailed distribution of trace fossils in three main successions.

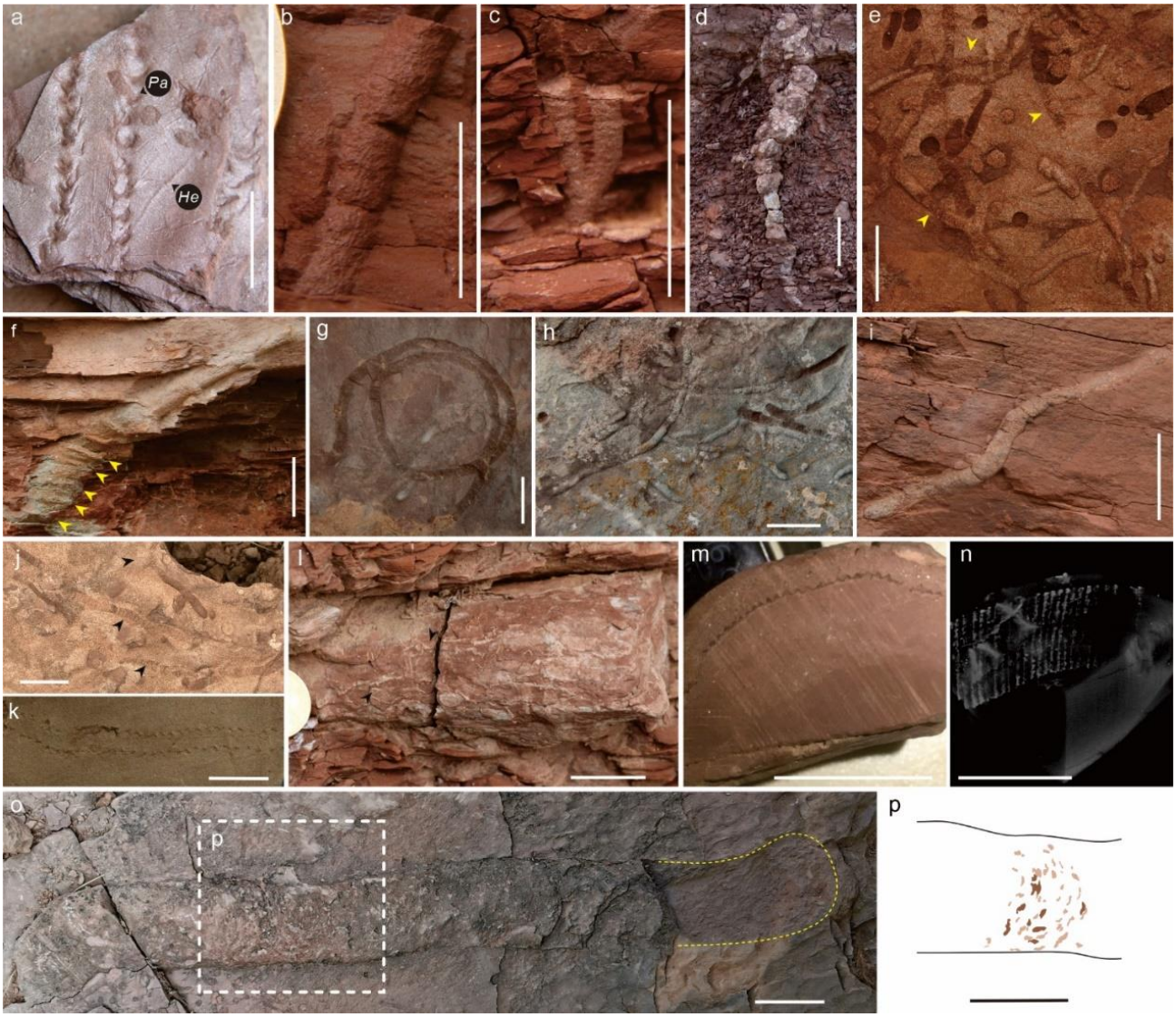

Figure 2. Ichnofossils from the Heshanggou Formation of North China. (a) Shallow tiers *Kouphichnium* and *Helminthoidichnites* (He) are crosscut by immediate tier *Palaeophycus* (Pa). (b) *Skolithos* cf. *serratus* with faint oblique striations. (c) Y-shaped *Psilonichnus* isp. (d) Downward unbranched and tapered rhizocretion. (e) Shallow tiers *Beaconites coronus*, arrows show tightly stacked arcuate meniscus. (f) *Camborygma* isp. shows enlarged terminal chamber and possible transverse scratches (arrows). (g) *Gordia* isp. with darker and finer infills. (h) High density *Palaeophycus tubularis* preserved on the sole of thick sandstone. (i) Inclined *Planolites beverleyensis* within siltstone. (j) *Taenidium barretti* (arrows) pass through the rippled surface. (k) Horizontal *Camborygma*, the outer surface is intertwined with tiny root traces (arrows). (l) Biserial

Diplichnites gouldi. (m–n) Internode cross-section of *Neocalamites* stem and micro-CT structure, showing the clear ribs and grooves. (o–p) Large ?*Beaconites* on top of rippled sandstone, rectangle in (p) shows meniscus-like portions comprising of gritty infillings. Scale bar of (d, f, h, o–p) are 40 mm, the rest are all 20 mm.

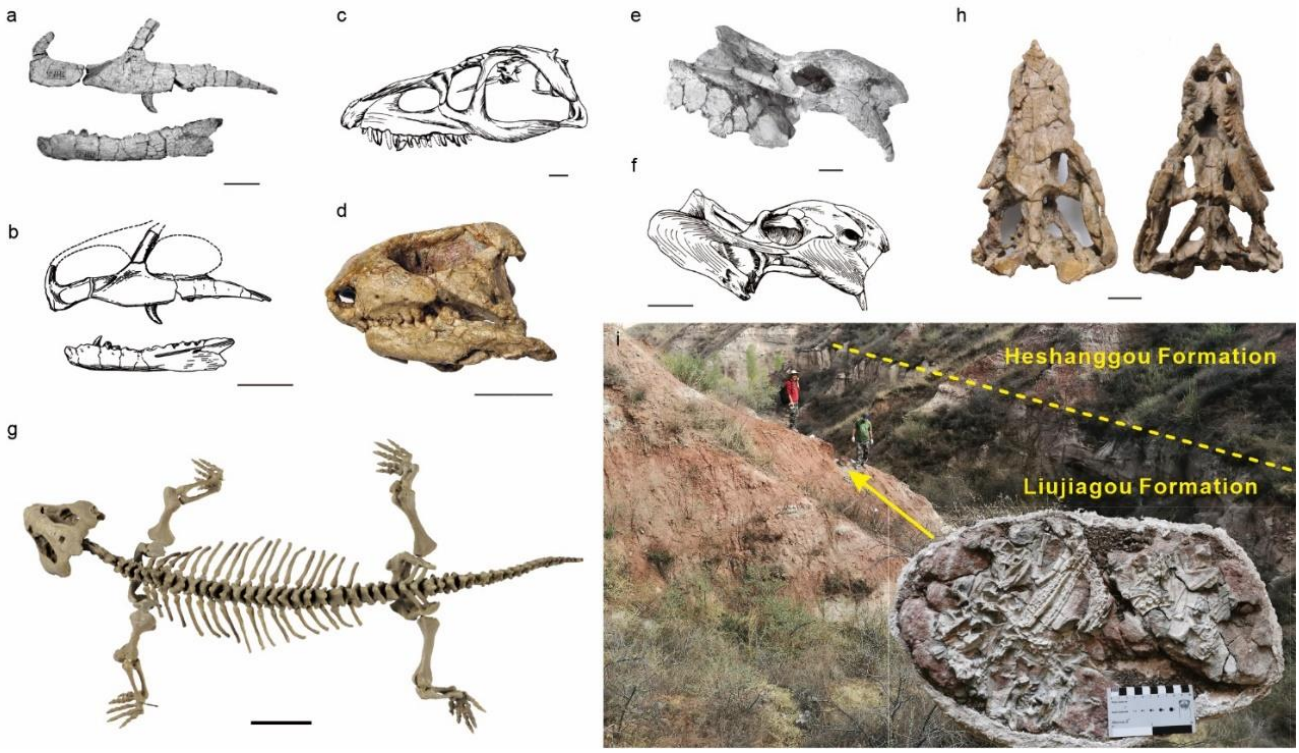

Figure 3. Vertebrates from the Heshanggou Formation of North China. (a–b) Skull elements of *Xilousuchus sapingensis* and drawings. (c) *Fugusuchus hejiapanensis*. (d) *Eumetabolodon bathycephalus*. (e–f) *Shaanbeikannemeyeria xilouensis* and drawing. (g) *Pentaedrusaurus ordosianus*. (h) *Hazhenia concava*, (i) Dashed line shows the boundary between the Liujiagou and Heshanggou formations. Arrow displays fossil horizon of the inserted picture at the base of the Heshanggou Formation. (b, c, f) are from Li et al. (2008). Scale bars are 40 mm.

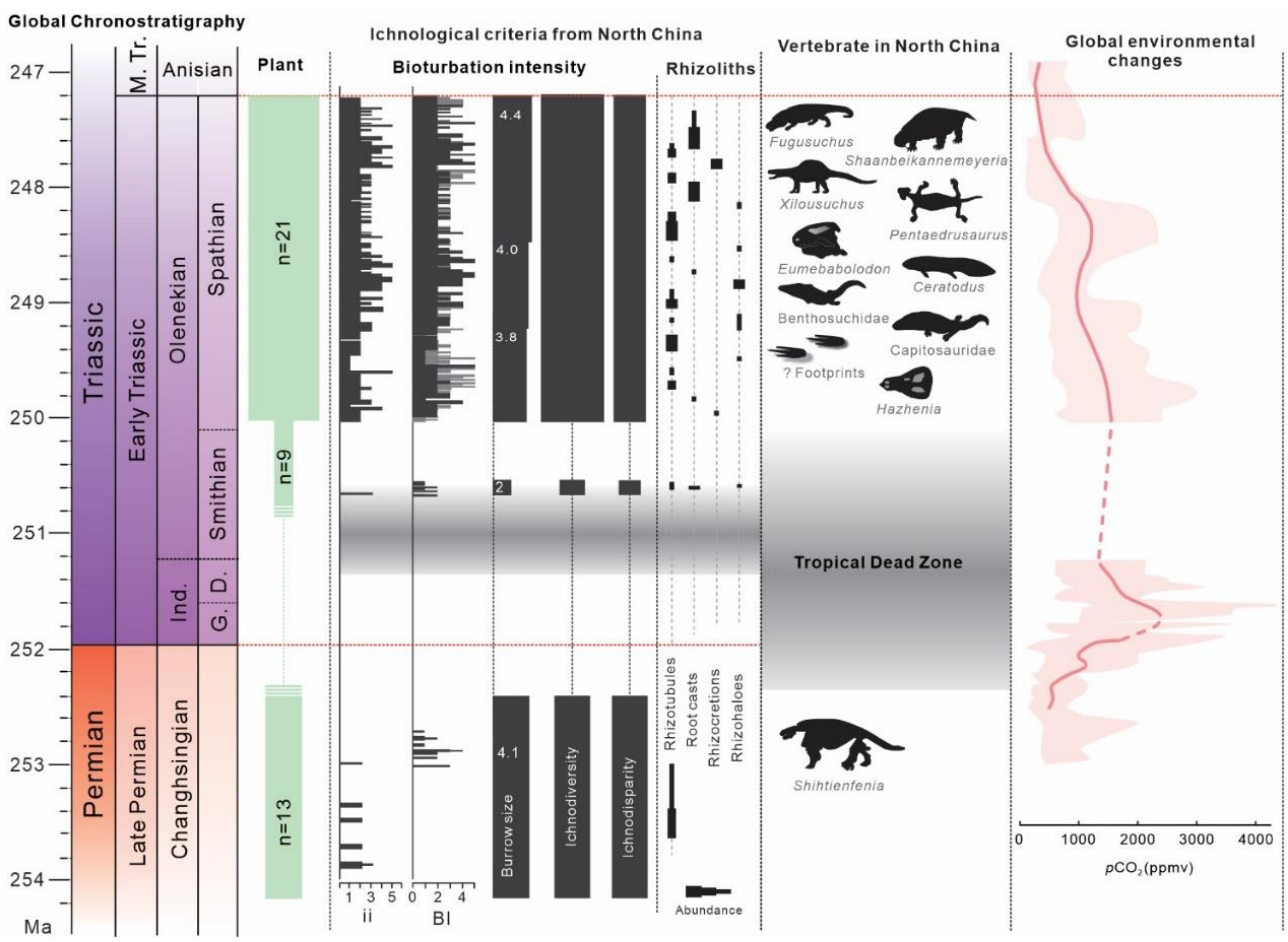

Figure 4. Ichnofossil data in North China and global terrestrial ecosystem changes from latest Permian to earliest Middle Triassic. Geochronological timescale is based on the latest version of the International Chronostratigraphic Chart (https://stratigraphy.org/). Plant richness from Shu et al. (2022). Numbers in Burrow size column represent the mean trace fossil sizes from the investigated interval. Drainage conditions of paleosols are inferred from preservation of rhizoliths and their relative depths. Ranges of microbially induced sedimentary structures (MISS) are from Chu et al. (2017). Atmospheric CO_2 curves are modified from Joachimski et al. (2022). Abbreviations: Ind. = Induan; G. = Griesbachian; D. = Dienerian.

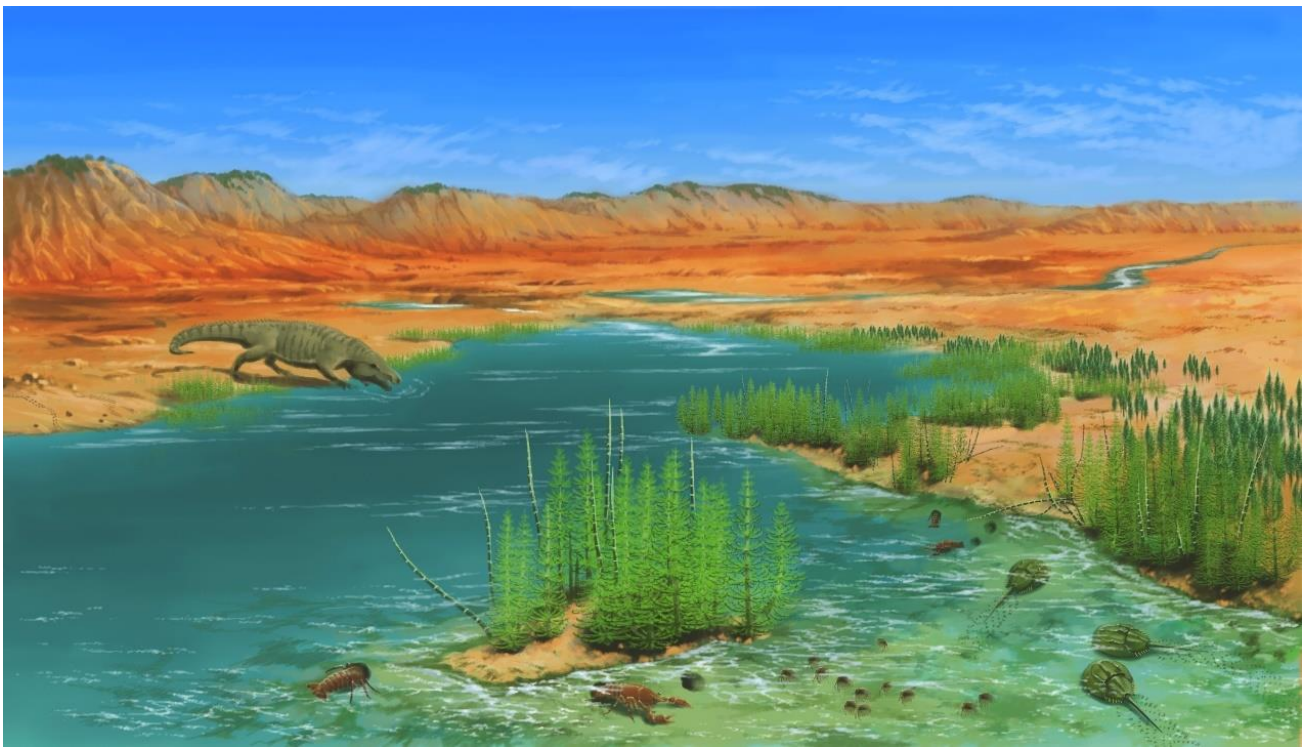

Figure 5. Reconstruction of the Spathian (Heshanggou Formation) coastal mudplain to alluvial ecosystem in North China. Plant communities in the coastal mudplain and alluvial facies are depauperate, dominated by *Neocalamites* and *Pleuromeia*, and only diverse at the top of the Heshanggou Formation (late Spathian; Shu et al., 2022). Fossil plants and tetrapods, coupled with diverse invertebrates, including limuloids, crayfish, spinicaudatans, and insects, etc., reveal reorganization of a relatively complex ecosystem in riverain region during the Spathian. The artistic illustration was credited by J. Sun.

Supplementary files for

Rapid tropical riparian ecosystem recovery in North China Basin following the end-Permian mass extinction

Wenwei Guo[1, 2], Li Tian[2*], Daoliang Chu[2], Wenchao Shu[2], Michael J. Benton[3], Jun Liu[4], and Jinnan Tong[2]

[1]College of Culture and Tourism, Zhangzhou Institute of Technology, Zhangzhou 363000, People's Republic of China.
[2]State Key Laboratory of Biogeology and Environmental Geology, China University of Geosciences, Wuhan, 430074, People's Republic of China.
[3]School of Earth Sciences, University of Bristol, BS8 1RJ, UK.
[4]Institute of Vertebrate Paleontology and Paleoanthropology, Chinese Academy of Sciences, Beijing 100044, People's Republic of China

Introduction

The Supplementary files include: (1) file 1: Early Triassic chronostratigraphic timescale in North China (Figures S1-2) and brief description of facies associations of the studied sections (Table S1); file 2: detailed description of traces fossils (Fig S3-6), fossil size variations (Figures S7-8), designations of ichnodiversity and tiering level (Tables S2-4) and possible trace producers on land (Table S5).

File 1. Integrated stratigraphic timescale and depositional environment

Detailed sedimentological investigations at the three studied sections have been undertaken by Ji et al. (2022) and Yu et al., (2022). Therefore, we primarily summarize the lithofacies and facies associations, and add more information about trace fossils (Figure S1 and Table S1).

Body fossil records in the red bed predominated Permian–Triassic transitional successions were too limited to establish a high-resolution timescale for global correlation. Based on the U-Pb CA-ID-TIMS age calibrated magnetostratigraphy from the Shichuanhe section (Guo et al., 2022), we complied other detrital zircon U-Pb ages during the Early Triassic, to provide a better constrained chronostratigraphy in North China (Zhu et al., 2019; 2022; Lu et al., 2022).

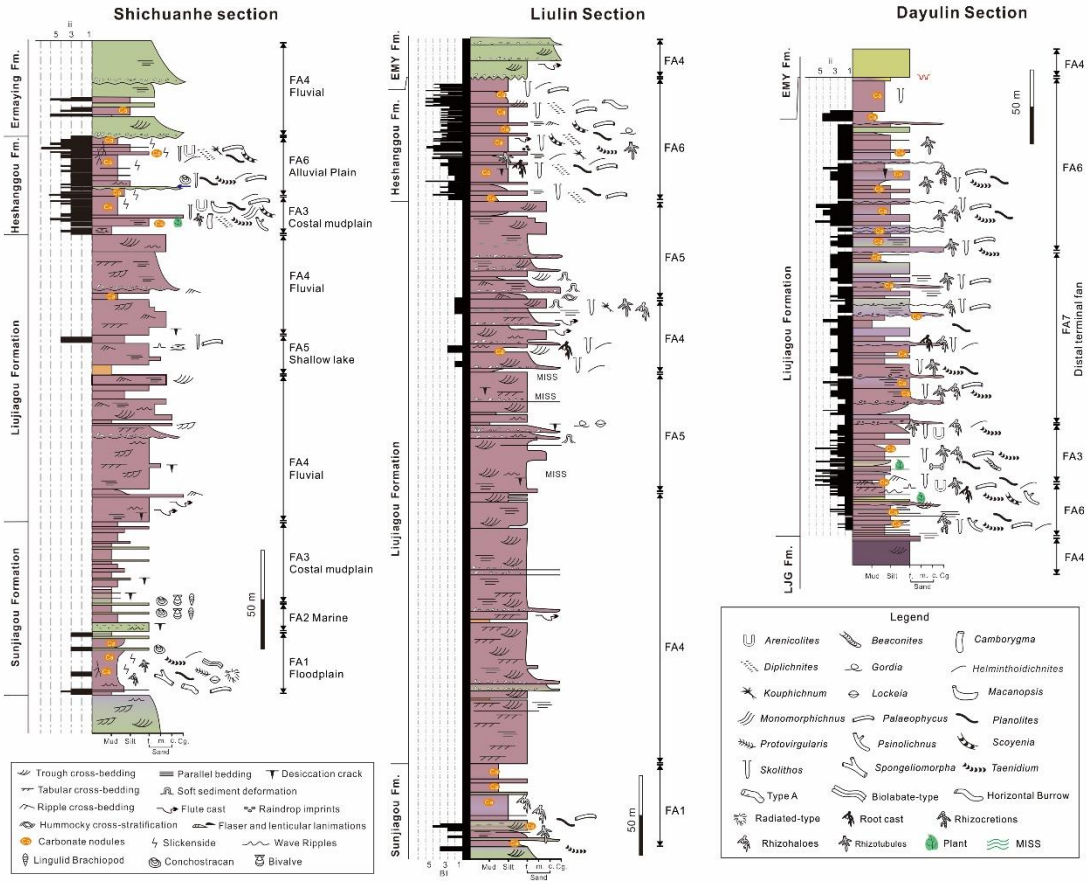

Figure S1. Lithology, sedimentology and ichnology of the studied sections.

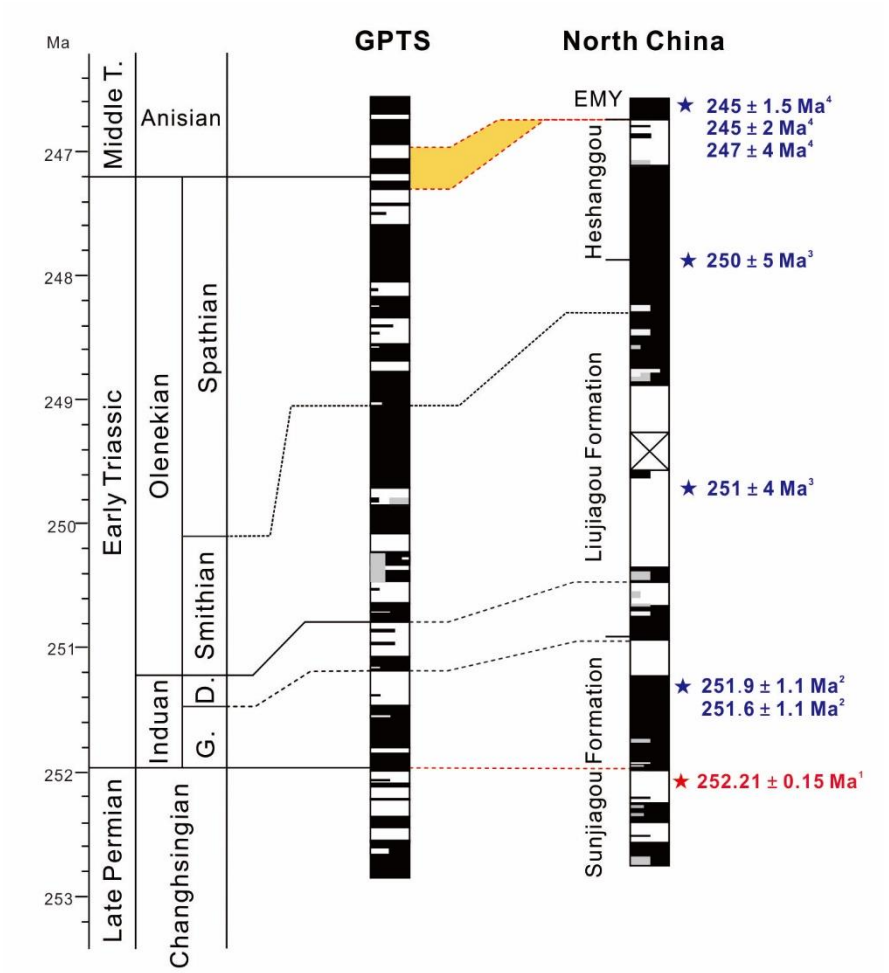

Figure S2. Early Triassic geochronological scale in North China. The Geo-magnetic polarity timescale (GPTS) is from Hounslow and Muttoni (2010) and Hounslow and Balabanov (2018). Magnetostratigraphy and the CA-ID-TIMS age of [1] are from Guo et al. (2022). Detrital zircon U-Pb ages are based on: [2] = tuffaceous claystones sampled from the uppermost part of the Sunjiagou Formation (Lu et al., 2022), [2] = around middle part of the Liujiagou Formation (Zhu et al., 2019), [3] = sandstone from the base of the Heshanggou Formation and tuffs from the bottom Ermaying Formation (EMY; Zhu et al., 2022). G. = Griesbachian, D. = Dienerian.

Table S1. Brief description of lithofacies, facies associations (FA) and trace fossils at the studied sections.

FA	Lithology	Trace fossils	Depositional environments
FA1	• Dominated by red mud-siltstone with paleosols (Msp) and interbedded with cross-bedded sandstone (Scb). • Well-developed paleosols in Msp, of moderate to very high maturity, contained layered calcareous nodules up to 10 cm in diameter, which were assigned to Aridisols and Vertisols.	• Root traces (Rh) and burrows (e.g., *Planolites* (*Pl*, *Taenidium* (*Ta*)) are common in Msp. • Scb is also bioturbated, especially at the Shichuanhe section. Diverse traces, including *Lockeia* (*Lo*), *Protovirgularis*, *Pa*, *Ta*, *Spongeliomorpha*, and several informally designated types have been identified. • Generally, animal traces are crosscut by roots.	• Distributed in the middle and upper Sunjiagou Formation. • **Arid floodplain.**
FA2	• Comprised of grayish-green silty mudstone (Ms), marine marls and calcareous sandstone. • A mixed continental-marine fauna, including conchostracans, bivalves, brachiopods and plant debris, have been identified (Chu et al., 2019).	No trace fossil found.	• Exclusively distributed in the lower Sunjiagou Formation of Shichuanhe section. • **Terrestrial facies with periodical marine flooding events**
FA3	• Comprise red Ms and Sandstone (S). • In upper Sunjiagou Formation, gypsum crystals, blocky calcite cements, Fe-oxide hypocoating occasionally occurred.	• Bioturbation is absent in the upper Sunjiagou Formation (Earliest Triassic). • Strata in the lower Heshanggou Formation (Spathian) are moderately reworked, several ichnogenera (e.g., *Pl*, *Palaeophycus* (*Pa*), *Beaconites* (*Be*), *Ta*), plant debris, root traces, and vertebrate	• Distributed in upper Sunjiagou and lower Heshanggou formations. • **Costal mudplain facies.**

		remains, have been identified.	
FA4	• Dominated by Pale red to grey purple Scb, planar-laminated sandstone (Sp), interbedded with thin dark red siltstone (Si), where Inceptisols are weakly- developed.	• *Kouphichnium* (*Kou*) (Shu et al., 2018) and tiny *Helminthoidichnites* have been found in Si. • Vertical burrows of *Skolithos* (*Sk*) and Rh, occurred occasionally in Scb, but the sediments were weakly bioturbated.	• Distributed in the Liujiagou and Ermaying formations. • **Low sinuosity fluvial system.**
FA5	• Consists of Scb, planar-laminated sandstone (Sp), hummocky and swaley cross-stratified sandstone (Sh), current and wave-rippled sandstone (Scr, Swr), interbedded with Intraformational conglomerate (Ci), which • Microbially induced sedimentary structures (MISS) are quite common, especially at Liulin Section (Chu et al., 2015, 2017).	• Depauperated ichnofauna, dominated by *Sk*, *Lo or Gordia*. • Bioturbation in this interval is weak.	• Distributed in the middle-upper Liujiagou Formation. • **Shallow lake and lake margin facies, with influence of major storm events.**
FA6	• Consists of dark red massive Msp, Scb, and Sp. • Sheetlike sandy bodies display lightly erosive bases.	• Msp contain diverse trace fossils, including *Kou*, *Diplichnites*, *Be*, *Ta*, *Camborygma*, *Psinolichnus* and various types of root traces, which moderately disturbed the sediments. • Trace fossils in sandstones are mainly *Sk*, *Pl* and Rh. • In several horizons, the top of several centimeters of the strata is strongly reworked.	• Heshanggou Formation. • **Alluvial plain with shallow lakes facies.**
FA7	• Dominated by massive sandstone with sharp base and trough cross-bedded or planar lamination, interlayered with dark red Msp and intraclast conglomerates, constituting several fining-upward	• Relatively simple ichnoassemblage, dominated by *Sk*, *Pa*, *Ta* and Rh • Root traces generally crosscut animal traces.	• In the Heshanggou Formation of Dayulin section. • **Distal terminal fan**

	sequences. • Vertisols and calcic Inceptisols, of low maturity, are well-developed in Msp.		**facies**

File 2. Ichnological information

In this section, all trace fossils encountered (Figures S2–5) and their size variations Figures S6–7) are provided. Ichnodisparity designation (Tables S2–4) follows Buatois et al. (2017). Traces from the Shichuanhe section have been documented by Guo et al. (2019), but several new ichnogenera have been found during the ongoing field seasons and are described here (Figure S3). Additionally, possible trace maker(s) on land are also discussed, based on paleontological and neoichnological evidence (Table S5). Accordingly, an artistic illustration of the early recovered ecosystem on land in North China have been reconstructed (Figure S8).

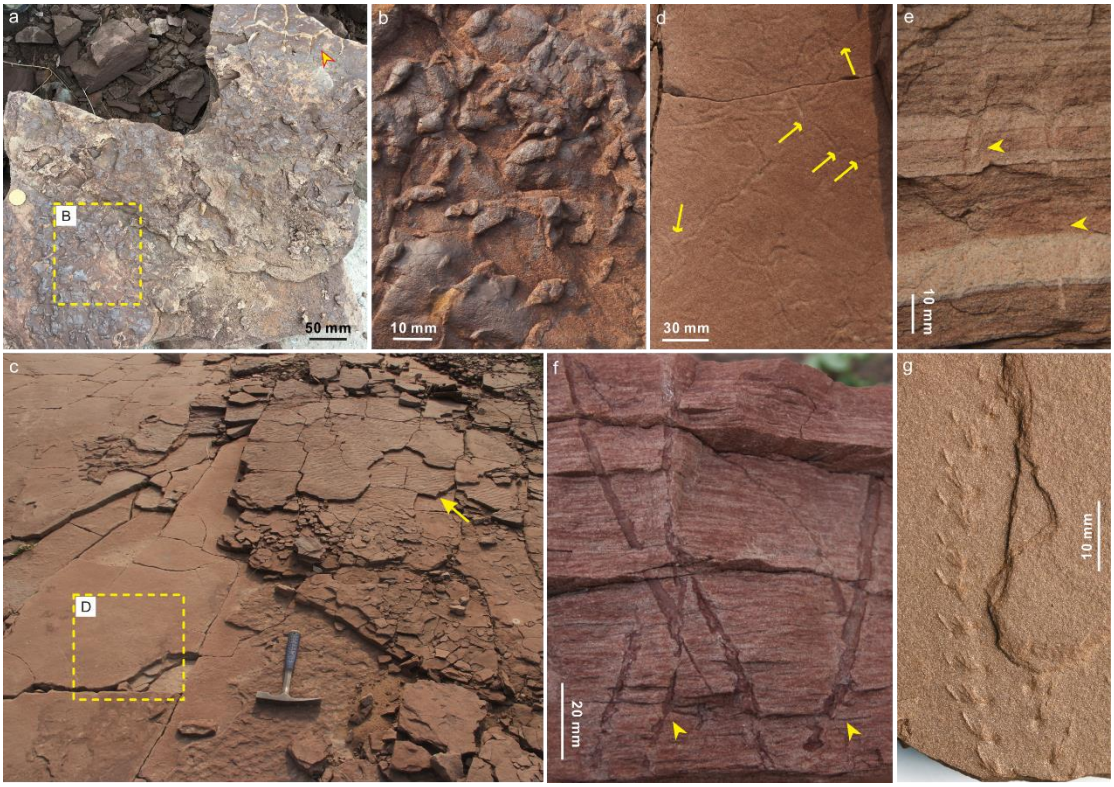

Figure S3. Ichnofauna from the Liujiagou Formation at Liulin section. (a-b) Ovate to elongated almond-shaped *Lockeia siliquaria* roughly arranged along a similar direction, fossils were preserved as convex hypichia in sandstone with desiccation cracks (arrow in a). (c-dd) Simple unbranched surficial burrows with sharp turns (arrows in d), self-overcrossing occasionally seen, traces are identified as *Gordia indianaensis* and preserved in rippled sandstone (arrow in c). (e) Vertical *Skolithos linearis* in sandstone. (f) Vertical root traces, showing inconsistent burrow sizes and tiny bifurcations (arrows). (g) *Kouphichnium didactylum* with simple foot imprints and a pusher imprint.

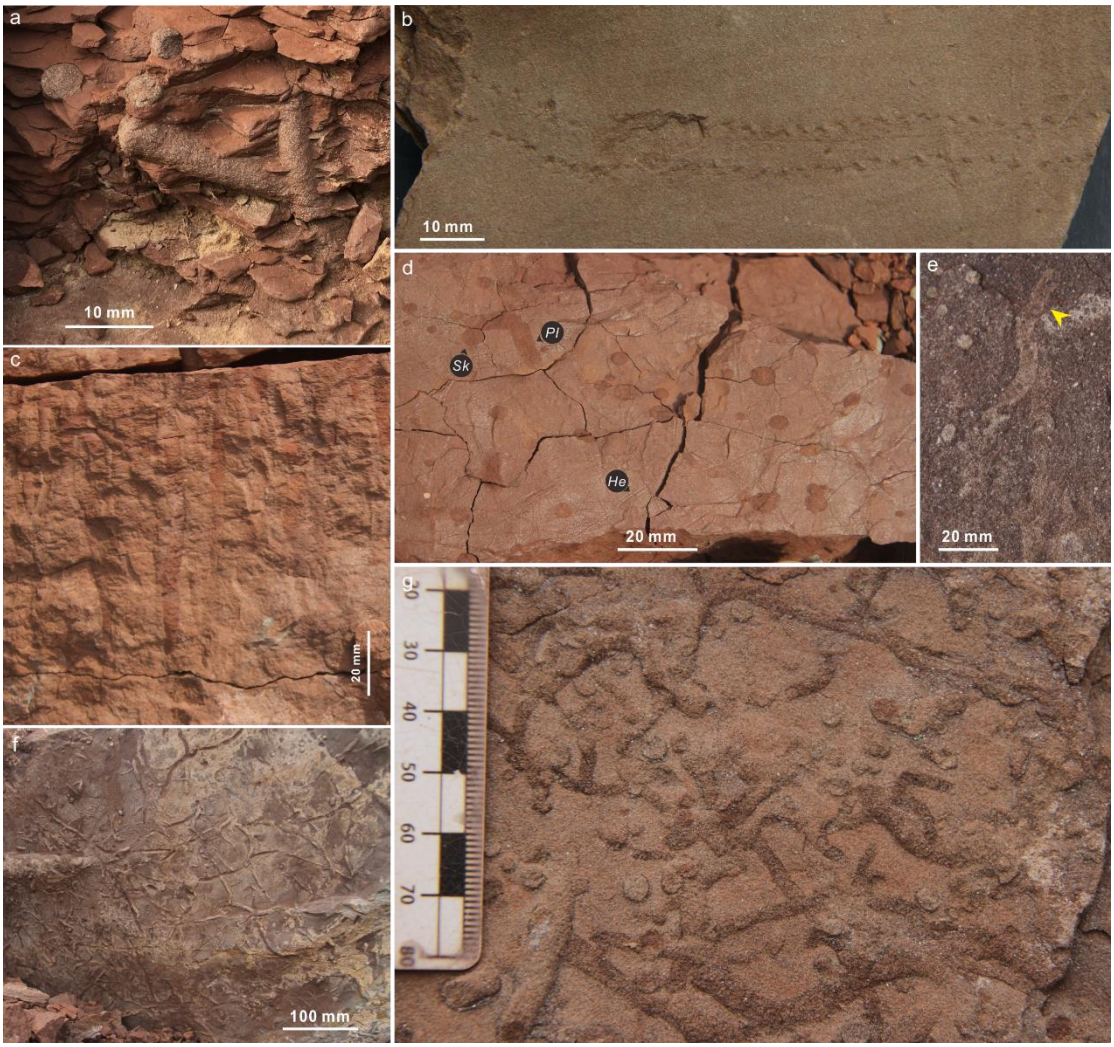

Figure S4. Ichnofauna from the Heshanggou Formation. (a) Y-shaped *Psilonichnus* cf. *upsilon*, the branch portion displays similar size with the main tube. FA3 costal mudplain facies at Shichuanhe section. (b) *Diplichnites gouldi*, evenly spaced imprints are comma or elongated and incline to the midline. Fossils preserved in FA3 at Shichuanhe section. (c) High-density simple vertical *Skolithos linearis* at Dayunlin section. (d) Actively filled *Planolites beverleyensis* (*Pl*) pass through surficial *Helminthoidichnites tenuis* (*He*), which in turn, crosscut by *Skolithos* (*Sk*). Dayunlin section. (e) Horizontal *Taenidium serpentinum*, distance between menisci (arrow) is roughly equal to the burrow width. Dayunlin section. (f) Crowded *Palaeophycus tubularis* preserved on the sole of thick sandstone. Liulin section. (g) Horizontal to inclined, straight to curve, lined *Beaconites coronus* with moderately arcuate menisci. Liulin section.

Figure S5. Large burrows from the Heshanggou Formation. (a-b) Horizontal but inclined unlined burrow with elliptical cross sections, branching and terminal chamber were no found. Possible lateral scratches could be seen on the side (Arrows in b). trace fossil is informally assigned to undesigned burrow. Liuin section. (c-e) Large ? *Beaconites* and other relatively small traces (e.g., *Palaeophycus*) on the rippled siltstone (ripple marks can be seen at the top-right of c). Burrows display meniscus-like portions, comprising of gritty infillings (Arrow in e), akin to *Beaconites* reported from breccia facies in the Devonian (Brück, 1987). Mafang outcrops. (f-h) Vertical to subhorizontal burrows with circular cross sections, filled with calcareous sand. Trace fossils are similar to crayfish burrows (*Camborygma*), although branches, terminal chamber or scratch marks were no found. Hongyatou outcrop. (i-j) In situ preserved *Neocalamites* stems in the lower part of the Heshanggou Formation at Shichuanhe section and Hongyatou outcrop, respectively. Typically, all the stems are associated with *Camborygma* and other burrows and trackways.

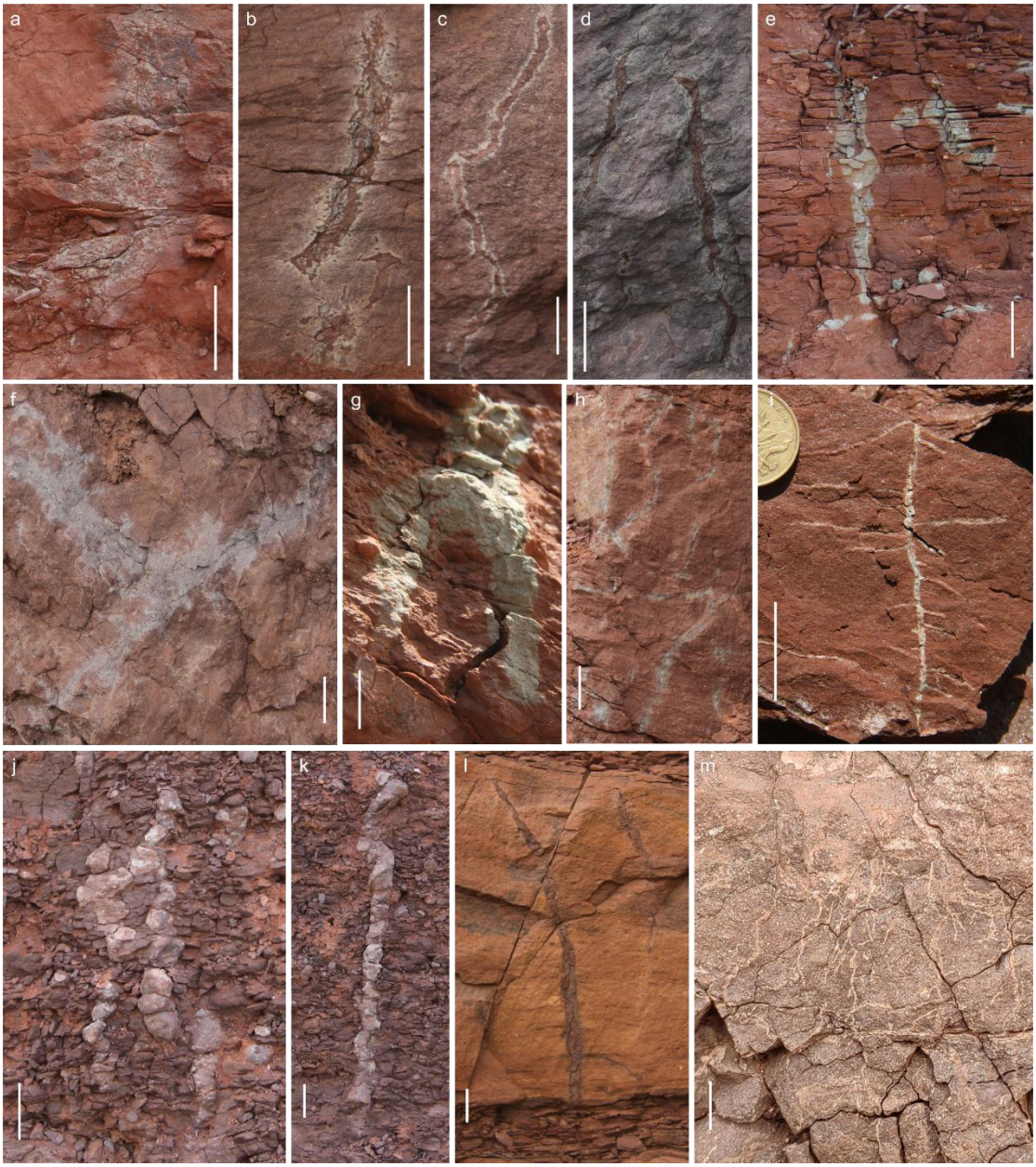

Figure S6. Root traces from the Heshanggou Formation in studied sections and outcrops. (a-h) Vertical branched rhizolith with green or pale purple haloes, showing irregular burrow sizes and lateral small rootlets (d, f), Yiyang section. (i) Herringbone-like branched rhizotubules, Yiyang section. (j-k) Vertical tapered unbranched or bifurcated rhiozocretions, Yiyang section. (l) Simple vertical branched roots, Tuncun outcrops. (m) Horizontal small rootlets, Yiyang section. Classification of root traces are based on Klappa (1980) and Kraus and Hasiotis (2006). All scale bars are 20 mm.

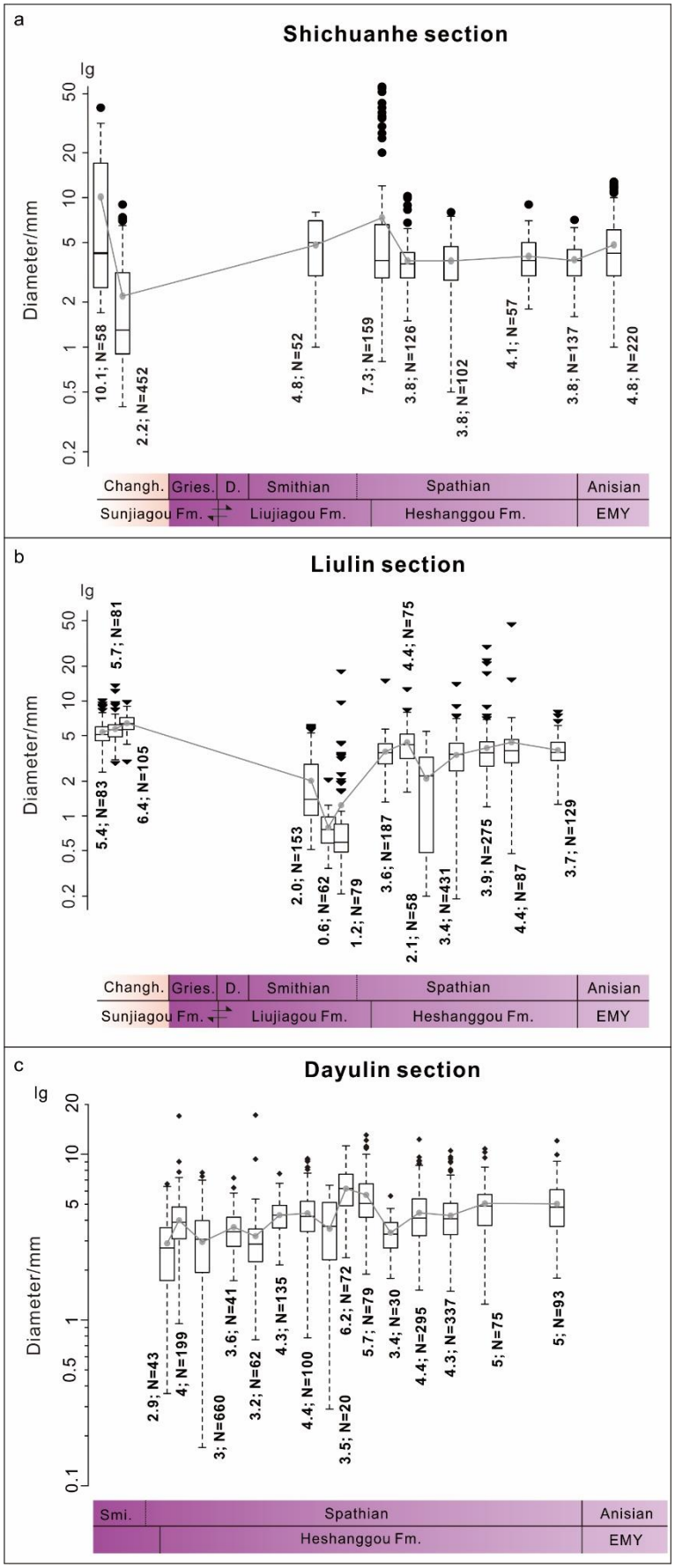

Figure S7. Size variation of all ichnogenera from there sections. EMY = Ermaying Formation.

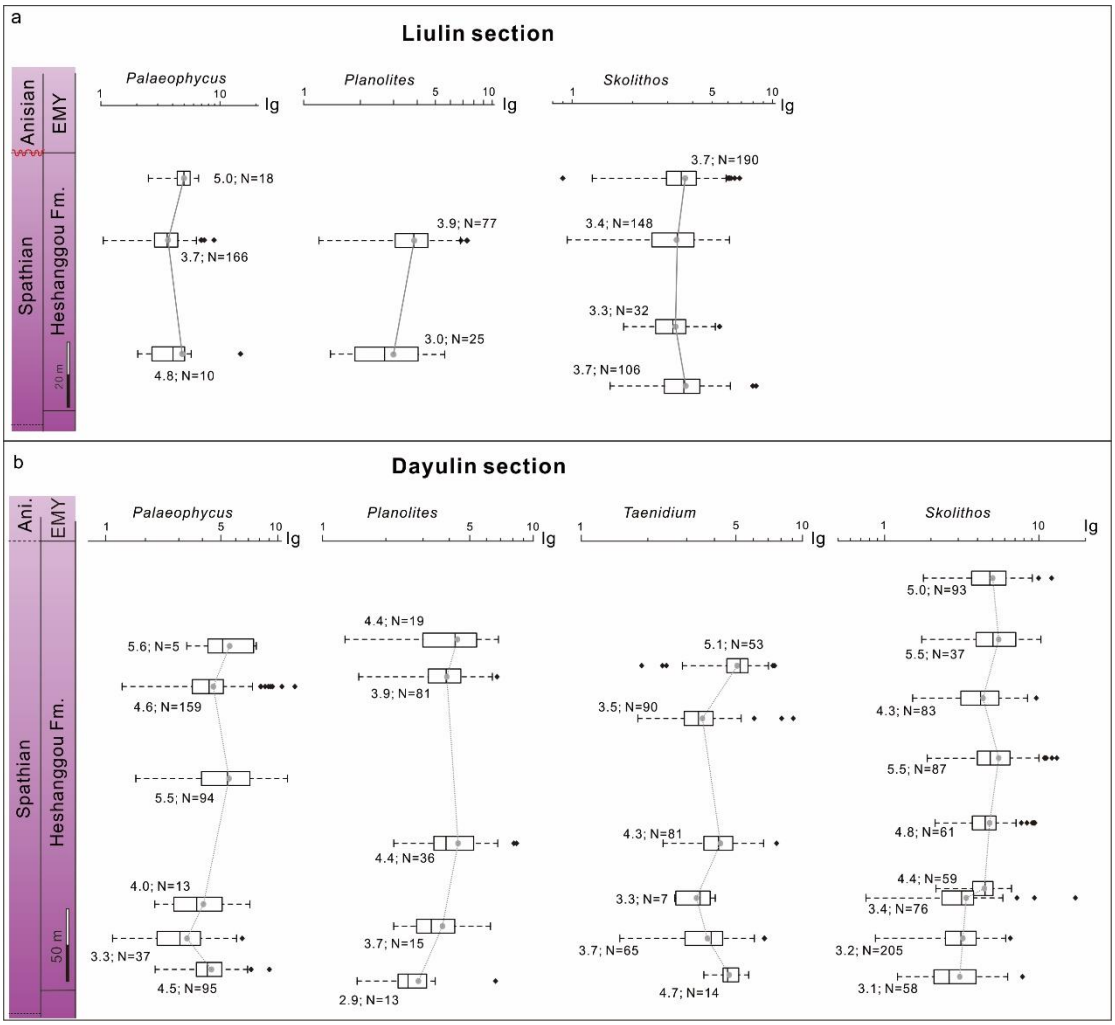

Figure S8. Size variation of sing ichnogenus from Liulin and Dayulin sections during the Spathian. EMY = Ermaying Formation.

Table S2. List of ichnogenera from the Shichuanhe section, Ichnodisparity designations and Tiering level.

	Ichnodisparity	Ichnogenus	Tier
Sunjiagou Formation	10-Passively filled horizontal burrows	*Palaeophycus*	Shallow-infaunal
	35-Vertical unbranched burrows	*Skolithos*	Deep -infaunal
	50-Maze and boxwork burrows	*Spongeliomorpha*	Shallow-infaunal
	12-Simple actively filled (meniscate) horizontal to oblique	*Taenidium*	Intermediate-infaunal
	1-Simple horizontal trails	*Helminthoidichnites*	Semi-infaunal
	3-Chevronate trails	*Protovirgularia*	Shallow-infaunal
	30-Isolated and serial oval to almond-shaped burrows	*Lockeia*	Semi-infaunal
	Rhizoliths	Rhizoliths	Deep-infaunal
Liujiagou Formation	10-Passively filled horizontal burrows	*Palaeophycus*	Shallow-infaunal
	35-Vertical unbranched burrows	*Skolithos*	Deep-infaunal
Heshanggou Formation	36-Vertical single U- and Y-shaped burrows	*Arenicolites*	Deep-infaunal
		Psilonichnus	Intermediate-infaunal
	52-Simple to complex burrows with terminal chambers	*Camborygma*	Deep-infaunal
		Macanopsis	Intermediate-infaunal
	1-Simple horizontal trails	*Helminthoidichnites*	Semi-infaunal
	6-Trackways and scratch imprints	*Diplichnites*	Surficial
		Monomorphichnus	Surficial
		Kouphichnium	Surficial
	10-Passively filled horizontal burrows	*Palaeophycus*	Shallow to Intermediate-infaunal
	11-Simple actively filled (massive) horizontal to oblique	*Planolites*	Intermediate-infaunal
	12-Simple actively filled (meniscate) horizontal to oblique	*Scoyenia*	Intermediate-infaunal
		Taenidium	Shallow-infaunal
	35-Vertical unbranched burrows	*Skolithos*	Deep-infaunal
	Rhizoliths	Rhizoliths	Deep-infaunal

Table S3. List of ichnogenera from the Heshanggou Formation of the Dayulin section, Ichnodisparity designations and tiering level.

	Ichnodisparity	Ichnogenus	Tier
Heshanggou Formation	1-Simple horizontal trails	*Helminthoidichnites*	Semi-infaunal
	10-Passively filled horizontal burrows	*Palaeophycus*	Shallow to Intermediate-infaunal
	11-Simple actively filled (massive) horizontal to oblique	*Planolites*	Intermediate to deep-infaunal
	12-Simple actively filled (meniscate) horizontal to oblique	*Taenidium*	Intermediate-infaunal
		Beaconites	Intermediate-infaunal
		Scoyenia	Intermediate-infaunal
	35-Vertical unbranched burrows	*Skolithos*	Deep-infaunal
	36-Vertical single U- and Y-shaped burrows	*Arenicolites*	Deep-infaunal
		Psilonichnus	Intermediate to deep-infaunal
	Rhizoliths	Rhizoliths	Deep-infaunal

Table S4. List of ichnogenera from the Liulin section, Ichnodisparity designations and tiering level.

	Ichnodisparity	Ichnogenus	Tier
Sunjiagou Formation	10-Passively filled horizontal burrows	*Palaeophycus*	semi-infaunal
	11-Simple actively filled (massive) horizontal to oblique	*Planolites*	Intermediate-infaunal
	12-Simple actively filled (meniscate) horizontal to oblique	*Taenidium*	semi-infaunal
	Rhizoliths	Rhizoliths	Deep-infaunal
Liujiagou Formation	1-Simple horizontal trails	*Helminthoidichnites*	Semi-infaunal
		Gordia	Semi-infaunal
	6-Trackways and scratch imprints	*Kouphichnium*	Surficial
	30-Isolated and serial oval to almond-shaped burrows	*Lockeia*	Shallow to Intermediate-infaunal
	Rhizoliths	Rhizoliths	Deep-infaunal
Heshanggou Formation	6-Trackways and scratch imprints	*Kouphichnium*	Surficial
		Diplichnites	Surficial
	10-Passively filled horizontal burrows	*Palaeophycus*	Shallow to Intermediate-infaunal
	11-Simple actively filled (massive) horizontal to oblique	*Planolites*	Intermediate-infaunal
	35-Vertical unbranched burrows	*Skolithos*	Deep-infaunal
	12-Simple actively filled (meniscate) horizontal to oblique	*Taenidium*	Intermediate-infaunal
		Beaconites	Intermediate-infaunal
	1-Simple horizontal trails	*Helminthoidichnites*	Semi-infaunal
		Gordia	Shallow-infaunal
	Rhizoliths	Rhizoliths	Deep-infaunal

Table S5. Possible trace producers on land.

Morphology	Ichnogenus	Intepretation
Simple horizontal trails	*Helminthoidichnites tenuis*	• Could be made by arthropods, vermiform animals, or insect larvae (Buatois et al., 1996, 1998).
Passively or actively filled burrow	*Palaeophycus*, *Planolites*	• Probably produced by insects or arthropods (Pemberton and Frey, 1982; Buatois and Mángano, 1993; Keighley and Pickerill, 1995).
Burrows with terminal chambers	*Camborygma*	• Freshwater crayfishes (Hasiotis and Mitchell, 1993; Hasiotis et al., 1993).
Vertical unbranched, single U- or Y-shaped burrows	*Skolithos*,	• Most of the *Skolithos* are smooth, but several specimens display distinct subvertical scratches. • arachnids, coleopterans, crickets, cicadas, bees or annelids can all build such burrows (Schlirf et al., 2001; do Nascimento and Netto, 2019).
	Arenicolites,	• Deeply extended with tiny tubes and wide limb distance. • Burrowed by polychaeta worms, crustaceans or may fly larvaes (Bromley, 1996; Rindsberg and Kopaska-Merkel, 2005).
	Psilonichnus	• Display similar sizes with branches, with bifurcation angle at 15°-45°. • Generally occurred in the Cenozoic marine facies, and constructed by decapod (Frey et al., 1984; de Carvalho, 2016). • Neoichnological investigations show that terrestrial arthropod, such as scorpion, can also produce similar Y-shaped burrows as temporary shelters or permanent dwellings (Hembree, 2016).
Backfilled burrows	*Beaconites* *Scoyenia* *Taenidium*	• Could be made by insects (cicadas, beetle larvaes), millipedes, oligochetes (earthworms) or vermiform on land, based on modern observations (Keighley and Pickerill, 1994; Rodríguez-Tovar et al., 2016; Boyd and McIlroy, 2017).
	? *Beaconites*	• Could be produced by either invertebrate, like arthropods and polychaete worms, or vertebrate, such as reptiles, amphibians (Brück, 1987; Allen and Williams, 1981; Morrissey and Braddy, 2004).
Trackways and scratch imprints	*Diplichnites* *Monomorphichnus*	• Could be left by myriapods or morphological similar arthropods (Bradshaw, 1981).
	Kouphichnium	• Limuloid (i.e., Shu et al., 2018).

References

Allen JRL, Williams BPJ. 1981. *Beaconites antarcticus*: a giant channel-associated trace fossil from the Lower Old Red Sandstone of South Wales and the Welsh Borders. *Geological Journal*, **16**: 255–269. https://doi.org/10.1002/gj.3350160405

Boyd C, McIlroy D. 2017. Three-Dimensional Morphology of *Beaconites capronus* from Northeast England. *Ichnos*, **24**: 250–258. doi: 10.1080/10420940.2017.1282862

Bradshaw MA. 1981. Paleoenvironmental interpretations and systematics of Devonian trace fossils from the Taylor Group (lower Beacon Supergroup), Antarctica. *New Zealand Journal of Geology and Geophysics*, **24**: 615–652. https://doi.org/10.1080/00288306.1981.10421537

Bromley RG. 1996. *Trace Fossils: Biology, Taxonomy and Applications*. London: Chapman & Hall.

Brück PM. 1987. A note on the trace fossil Beaconites barretti in the Old Red Sandstone of County Dublin, Ireland. *Proceedings of the Geologists' Association*, **98**: 259–263. https://doi.org/10.1016/S0016-7878(87)80043-3

Buatois LA, Mángano MG. 1993. Trace fossils from a Carboniferous turbiditic lake: implications for the recognition of additional nonmarine ichnofacies. *Ichnos*, **2**: 237–258. doi: 10.1080/10420949309380098

Buatois LA, Mángano MG, Wu XT, Zhang GC. 1996. Trace fossils from Jurassic lacustrine turbidites of the Anyao Formation (central China) and their environmental and evolutionary significance. *Ichnos*, **4**: 287–303. doi: 10.1080/10420949609380137

Buatois LA, Mángano MG, Maples G, Lanier WP. 1998. Ichnology of an upper Carboniferous fluvio-estuarine paleovalley: The Tonganoxie sandstone, Buildex quarry, eastern Kansas, USA. *Journal of Paleontology*, **72**: 152–180. doi: 10.1017/S0022336000024094

Buatois LA, Wisshak M, Wilson MA, Mángano MG. 2017. Categories of architectural designs in trace fossils: a measure of ichnodisparity. *Earth-Science Reviews*, **164**: 102–181. https://doi.org/10.1016/j.earscirev.2016.08.009

Chu DL, Tong JN, Song HJ, Benton MJ, Bottjer DJ, Song HY, Tian L. 2015. Early Triassic wrinkle structures on land: stressed environments and oases for life. *Scientific Reports*, **5**: 10109, https://doi.org/10.1038/srep10109.

Chu DL, Tong JN, Bottjer DJ, Song HJ, Song HY, Benton MJ, Tian L, Guo WW. 2017. Microbial mats in the terrestrial Lower Triassic of North China and implications for the Permian–Triassic mass extinction. *Palaeogeography*, *Palaeoclimatology*, *Palaeoecology*, **474**: 214–231. https://doi.org/10.1016/j.palaeo.2016.06.013

Chu DL, Tong JN, Benton MJ, Yu JX, Huang YF. 2019. Mixed continental-marine biotas following the Permian-Triassic mass extinction in South and North China. *Palaeogeography*, *Palaeoclimatology*, *Palaeoecology*, 519: 95–107. https://doi.org/10.1016/j.palaeo.2017.10.028

de Carvalho CN. 2016. *Psilonichnus* Fürsich, 1981 in its type-locality (Praia do Salgado, western Portugal). *Comunicaçõe Geológicas*, **103**: 13–21.

do Nascimento DL, Netto RG. 2019. *Skolithos serratus* in paleosols: Paleobiological, paleoecological, and paleobiogeographical insights. *Palaeogeography*, *Palaeoclimatology*, *Palaeoecology*, **530**: 152–162. https://doi.org/10.1016/j.palaeo.2019.05.044

Frey RW, Curran HA, Pemberton SG. 1984. Tracemaking activities of crabs and their environmental significance: the ichnogenus *Psilonichnus*. *Journal of Paleontology*, **58**: 333–350.

Guo WW, Tong JN, Tian L, Chu DL, Bottjer DJ, Shu WC, Ji KX. 2019. Secular variations of ichnofossils from the terrestrial Late Permian-Middle Triassic succession at the Shichuanhe section in Shaanxi Province, North China. Global and Planetary Change, 181: 102978. https://doi.org/10.1016/j.gloplacha.2019.102978

Guo WW, Tong JN, He Q, Hounslow MW, Song HY, Dal Corso J, Wignall PB, Ramezani J, Tian L, Chu DL. 2022.

Late Permian–Middle Triassic magnetostratigraphy in North China and its implications for terrestrial-marine correlations. Earth and Planetary Science Letters, 585: 117519. https://doi.org/10.1016/j.epsl.2022.117519

Hasiotis ST, Mitchell CE. 1993. A comparison of crayfish burrow morphologies: Triassic and Holocene fossil, paleo-and neo-ichnological evidence, and the identification of their burrowing signatures. *Ichnos*, **2**: 291–314. https://doi.org/10.1080/10420949309380104

Hasiotis ST, Mitchell CE, Dubiel RF. 1993. Application of morphologic burrow interpretations to discern continental burrow architects: lungfish or crayfish? *Ichnos*, **2**: 315–333. https://doi.org/10.1080/10420949309380105

Hembree D. 2016. Using experimental neoichnology and quantitative analyses to improve the interpretation of continental trace fossils. *Ichnos*, **23**: 262–297. https://doi.org/10.1080/10420940.2016.1202684.

Hounslow MW, Balabanov YP. 2018. A geomagnetic polarity timescale for the Permian, calibrated to stage boundaries. *Geological Society, London, Special Publications*, **450**: 61–103. https://doi.org/10.1144/SP450.8

Hounslow MW, Muttoni G. 2010. The geomagnetic polarity timescale for the Triassic: linkage to stage boundary definitions. *Geological Society, London, Special Publications*, **334**: 61–102. https://doi.org/10.1144/SP334.4

Ji KX, Wignall PB, Tong JN, Yu YY, Guo WW, Shu WC, Chu DL. 2022. Sedimentology of the latest Permian to Early Triassic in the terrestrial settings of the North China Basin: Low-latitude climate change during a warming-driven crisis. *Geological Society of America Bulletin*, **135**: 481-503. https://doi.org/10.1130/b36260.1

Keighley DG, Pickerill RK. 1994. The ichnogenus *Beaconites* and its distinction from *Ancorichnus* and *Taenidium*. *Palaeontology*, **37**: 305–338.

Keighley DG, Pickerill RK. 1995. Commentary: the ichnotaxa *Palaeophycus* and *Planolites*: historical perspectives and recommendations. *Ichnos*, **3**: 301–309. doi: 10.1080/10420949509386400

Klappa CF. 1980. Rhizoliths in terrestrial carbonates: classification, recognition, genesis and significance. *Sedimentology*, **27**: 613–629. https://doi.org/10.1111/j.1365-3091.1980.tb01651.x.

Kraus MJ, Hasiotis ST. 2006. Significance of Different Modes of Rhizolith Preservation to Interpreting Paleoenvironmental and Paleohydrologic Settings: Examples from Paleogene Paleosols, Bighorn Basin, Wyoming, U.S.A. *Journal of Sedimentary Research*, **76**: 633–646. https://doi.org/10.2110/jsr.2006.052

Lu J, Wang Y, Yang M, Zhang P, Bond DPG, Shao L, Hilton J. 2022. Diachronous end-Permian terrestrial ecosystem collapse with its origin in wildfires. *Palaeogeography, Palaeoclimatology, Palaeoecology*, **594**: 110960. https://doi.org/10.1016/j.palaeo.2022.110960

Morrissey LB, Braddy SJ. 2004. Terrestrial trace fossils from the Lower Old Red Sandstone, southwest Wales. *Geological Journal*, **39**: 315–336. https://doi.org/10.1002/gj.991

Pemberton SG, Frey RW. 1982. Trace fossil nomenclature and the *Planolites-Palaeophycus* dilemma. *Journal of Paleontology*, **56**: 843–881.

Rindsberg AK, Kopaska-Merkel DC. 2005. *Treptichnus* and *Arenicolites* from the Steven C. Minkin paleozoic footprint site (Langsettian, Alabama, USA). *Pennsylvanian Footprints in the Black Warrior Basin of Alabama*, **1**: 121–141.

Rodríguez-Tovar FJ, Alcalá L, Cobos A. 2016. *Taenidium* at the lower Barremian El Hoyo dinosaur tracksite (Teruel, Spain): Assessing palaeoenvironmental conditions for the invertebrate community. *Cretaceous Research*, **65**: 48–58. https://doi.org/10.1016/j.cretres.2016.04.013.

Schlirf M, Uchman A, Kümmel M. 2001. Upper Triassic (Keuper) non-marine trace fossils from the Haßberge area (Franconia, south-eastern Germany). *Paläontologische Zeitschrift*, **75**: 71–96. https://doi.org/10.1007/BF03022599

Shu WC, Tong JN, Tian L, Benton MJ, Chu DL, Yu JX, Guo WW. 2018. Limuloid trackways from Permian–

Triassic continental successions of North China. Palaeogeography, Palaeoclimatology, Palaeoecology, 508: 71–90. https://doi.org/10.1016/j.palaeo.2018.07.022

Shu WC, Tong JN, Yu JX, Hilton J, Benton MJ, Shi X, Diez JB, Wignall PB, Chu DL, Tian L, Yi, ZX, Mao YD. 2022. Permian−Middle Triassic floral succession in North China and implications for the great transition of continental ecosystems. Geological Society of America Bulletin, 135: 1747–1767. https://doi.org/10.1130/B36316.1

Yu YY, Tian L, Chu DL, Song HY, Guo WW, Tong JN. 2022. Latest Permian–Early Triassic paleoclimatic reconstruction by sedimentary and isotopic analyses of paleosols from the Shichuanhe section in central North China Basin. Palaeogeography, Palaeoclimatology, Palaeoecology, 585: 110726. https://doi.org/10.1016/j.palaeo.2021.110726

Zhu ZC, Liu YQ, Kuang HW, Benton MJ, Newell AJ, Xu H, An W, Ji SA, Xu SC, Peng N, Zhai QG. 2019. Altered fluvial patterns in North China indicate rapid climate change linked to the Permian-Triassic mass extinction. Scientific Reports, 9: 16818. https://doi.org/10.1038/s41598-019-53321-z

Zhu ZC, Liu YQ, Kuang HW, Newell AJ, Peng N, Cui MM, Benton MJ. 2022. Improving paleoenvironment in North China aided Triassic biotic recovery on land following the end-Permian mass extinction. Global and Planetary Change, 216: 103914. https://doi.org/10.1016/j.gloplacha.2022.103914